THE UNIVERSITY OF NEW SOUTH WALES

SCHOOL OF MECHANICAL AND MANUFACTURING ENGINEERING

THE STABILITY AND HANDLING CHARACTERISTICS OF BICYCLES

David Stevens

3135047

BACHELOR OF MECHANICAL ENGINEERING

June 2009

Supervisor: Dr. Nathan Kinkaid

Abstract

Developments have recently been made in analysis of bicycle self stability. Applicability of benchmarked linearized dynamics equations to a variation of modern bicycle designs is investigated. Results gained through experimentation on an instrumented bicycle with variable geometry are compared to predicted results. Precise three dimensional modeling is used to calculate bicycle mass properties, for use in dynamics equations. Strong correlations between experimental and predicted results are found over large variations in bicycle geometry.

Declaration

I, David Stevens, declare that this thesis is my own work, except where acknowledge, and has not been previously submitted for academic credit.

Acknowledgements

Over the course of writing this thesis, my supervisor Dr Nathan Kinkaid has offered support when it was needed, as well as technical advice. Your enthusiasm towards the project has been a great motivation throughout the year

Russell Overhall has been generous in passing on his experience, and knowledge. Thank you for having trust in my decision to attach your computer to my uncontrolled bicycle.

I would like to thank my girlfriend, friends and family, in particular my parents, for their support and encouragement throughout my education.

Table of Contents

Table of Figures

1 Introduction

Bicycles have remained a prominent part of society since their inception in the 1860s. The basic safety bicycle design has evolved in several directions which are commercially successful today. The market is dominated by road and track bikes, commuter bikes and mountain bikes. (Herlihy, 2004)

This thesis focuses on the variations in design of popular modern bicycles, and their influence on stability and handling characteristics. The handling properties of a bicycle are significant in how safe it is to ride, as well as how difficult it is to learn to ride on. While handling properties as felt by the rider are subjective, predictions may be made through knowledge of dynamic properties, particular those related to stability.

Through more than a century of development, successful bicycle configurations have been reached. However, much of this development has been through a process of evolution, rather than application of sound mathematic knowledge.

While variations exist in modern bicycle design, basic layouts remain similar across popular styles.

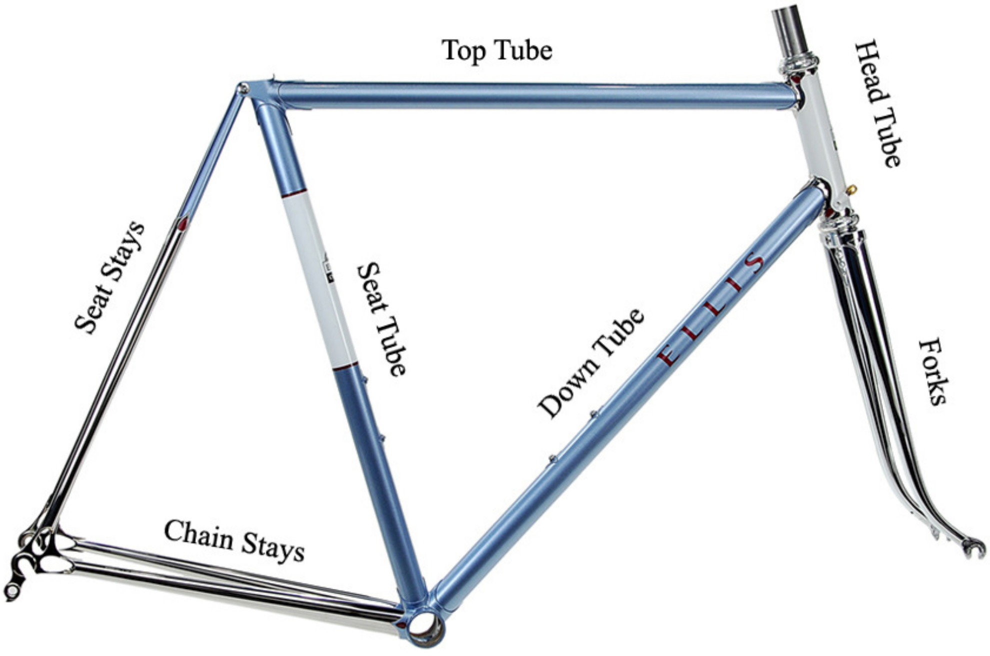

Figure 1: Frame Components Layout, Ellis 953 Road Frame (elliscycles.com)

Variations in any of the above components will affect dynamics of the bicycle. Most lengths and angles in a frame are interdependent, that is, one variation in component design will necessitate another. Wilson et al, (2004), states that the influence of trail is the most noticeable design characteristic to the rider.

Figure 2 Head Angle and Trail, on a Surly Steamroller, (surly.com).

Trail varies with alterations to head angles, wheel diameter, fork length and shape. The contrast in these parameters is clear across modern style of bicycle.

The road racing or track style bicycle in Figure 2 shows a steep head angle, and relatively short trail. Paterek (1985) describes the feeling of handling produced by steep head angles as stiff. This style of bicycle makes sacrifices in stability, to make gains in responsiveness to rider input.

The commuter or comfort style of bicycle in Figure 3 has a more relaxed head angle, as well as greater mechanic trail, due to the increased rake, or curve, in the forks. This style of bicycle offers comfortable riding with minimal rider input to maintain stability.

Figure 3 Commuter Bike, Giant Explorer (giant-bicycles.com)

In the most extreme instance, the downhill mountain bike shown in Figure 4 has a dramatically reduced head tube angle. Disregarding suspension, the geometric design aims to offer stability at high speed, through a resilient front end over rough terrain, minimizing effect of disturbances to steering angle by rocks and surface irregularities. (Paterek, 1985)

Figure 4 Downhill Mountain Bike, Mongoose EC-D (mongoose.com)

2 Bicycle Research History

Bicycles have been the subject of much research throughout their development. This thesis studies self stability of bicycles, which until recently had not been completely captured and verified mathematically. The work of Meijaard et al (2006), which produced a benchmarked set of dynamics equations, is the definitive resource for stability analysis.

While qualitative analysis of bicycle dynamics has been undertaken since as early as 1869, with Rankine introducing countersteer, most papers did not contain explanation for the ability of a bicycle to remain upright uncontrolled. In 1896 Sharp discussed stability without steering input, but explained that it was due to rider lean inputs, inducing steer through gyroscopic precession of the front wheel.

A significant paper dispelling some stability myths was that of Jones, published in 1970. Through a series of attempts at building an “unrideable bicycle” he dispelled the common belief that a bicycle’s stability is due entirely to gyroscopic precession of the front wheel. He also demonstrated instability of a bicycle with negative trail. Jones’ paper lacked mathematical theory to support his findings.

Significant research prior to that of Meijaard et al, in relation to development of dynamics equations, began in 1897 with Emmanuel Carvallo’s paper on bicycles, introducing mathematically the concepts of countersteer to initiate turns, and the importance of trail in stability. The absence of front frame inertia is the major short fall of Carvallo’s work, which has otherwise been proven correct, and included eigenvalue analysis leading to stable speed ranges.

Whipple's paper of 1899 presents non linear analysis of a bicycle, with minor errors, which become irrelevant when the expressions found are linearized. Whipple was the first to derive equations to describe the motion of a bicycle, and explain how a bicycle could balance itself under the right conditions. His work included the development of the Whipple Bicycle Model, consisting of four rigid laterally symmetrical parts connected by ideal hinges. Parts are front frame, rear frame, front wheel and rear wheel. This model is used by the Meijaard et al, 2006.

Somerfield, and Klein (1903) used Newtonian physics to analyze the front and rear frames. The paper was written in German, but the translation begins with the statement that the bicycle is in unstable equilibrium and must be learnt to ride. The paper focused on the role of the front wheel as a gyroscope in maintaining stability. The significance of this effect is not as great as was thought at the time. The equations derived agree with those of Dohring, 1955, (according to Meijaard et al, 2006), who presented the first correct equations of the Whipple model presented in open literature. This work included eigenvalue stability analysis on two motorcycles and a scooter.

In 1967, Neımark and Fufaev presented a book on non holonomic dynamics, featuring a derivation of the equation of motion of the Whipple bicycle model. In discussing this paper, Meijaard et al, (2006), write the equations derived show self stability, when the included steering stem friction term in sufficiently large. The paper had error and lack factors contributing to stability

In the 1970s, the Cornell Aeronautics Laboratory ran a research program on bicycles and motorcycles, resulting in 20 papers being produced. In particular, Rice and Roland's 1970 paper is the first to introduced the concept of mechanical trail, seen in Figure 2. Their model also included tyre slip and rider lean, giving a 8x8 first order equation.

The terms weave and capsize were first used in 1971 by Sharp, R., describing the unstable region of eigenvalues. His equations allow the vertical ground force on the front wheel to do work on the bicycle, and as such, his linearized equations are approximations only. It has since been show that this paper featured several typographical and algebraic errors.

In 1979, Psiaki wrote an undergraduate honors thesis describing motion for a bicycle with an upright rider, and a forward leaning rider, in no hands steer. Equations of motions were agree with later work of Meijaard et al (2006).

Equations of moments written in compact notation were written by Papadopoulos, (1987), also a coauthor of the Meijaard et al (2006) paper.

Hand's 1988 Cornell M.Sc thesis comprehensively compares previous literature, finding several agreeing equations. His own equations neglected terms in the Lagrangian, which drop out in linearization.

In 2004 Schwab, Meijaard, and Papadopoulos write a draft of the benchmark study on which this project is based, and present it at a conference. This work is review by Astrom, Klein, and Lennartsson in 2005, who also partake in a parameter study based on Schwab (2004) and Papadopoulos (1987). The majority of their work was based on super stable bike for teaching disabled children to ride.

An experimental validation of Meijaard et al’s benchmark equation was carried in 2006 (Kooijman, J. D.). This experiment featured an instrumented bicycle, and showed agreement with equations in the range of 2m/s to 6m/s. An inverted front fork was used to greatly increase trail, and produce stability a lower range of speeds. A regular bicycle configuration was not tested.

2.1 Linearized Dynamics Equation for Bicycles

Meijaard, Papadopoulos, Ruina, Schwab 2006

In 2006, J.P. Meijaard et al published the paper, “Linearized dynamic equations fro the balance and steet of a bicycle: a benchmark and review”. This presents canonical linearized equations of motion for the bicycle. Derivation is carried out by hand in two ways, and is checked against two non-linear dynamics simulations. The paper conducts a complete review of past literature, concluding that there was no previous peer reviewed paper written in English that presents complete and correct dynamic equations for the Whipple bicycle model (Figure 5).

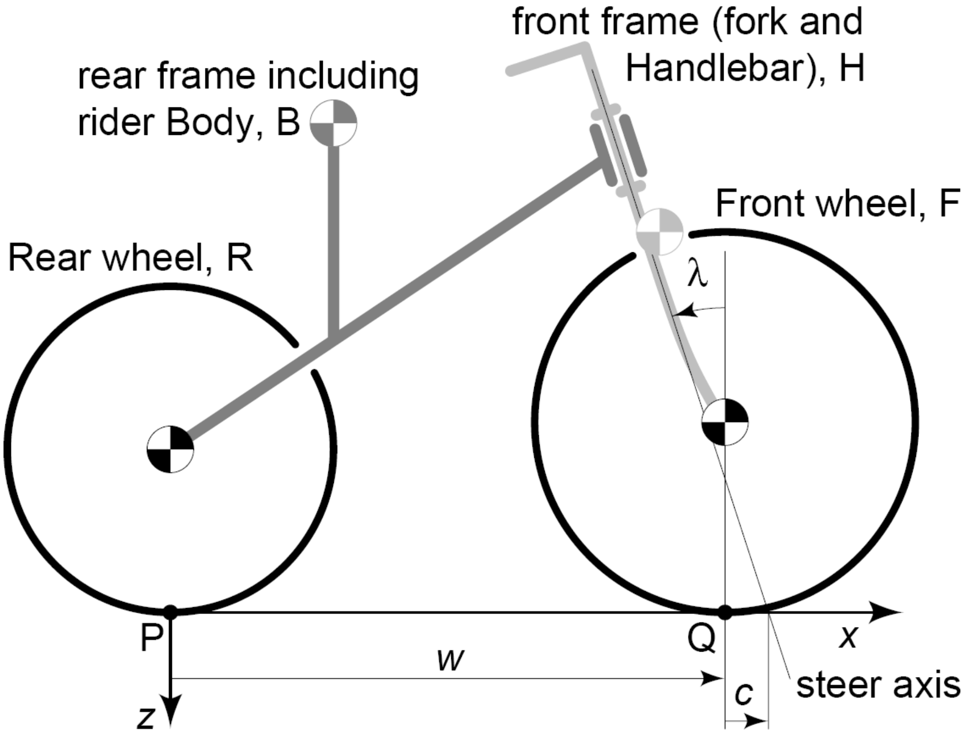

Figure 5 Bicycle Model (Meijaard, 2006)

Meijaard et al derive equations for the Whipple bicycle model, represented as follows. The model consists of four rigid bodies: a rear wheel R, a rear frame and rider body combined as B, a fork and handlebar assembly combined as H and a front wheel F. The model has symmetry between left and right sides. Ideal assumptions used are knife edge rolling contact rather than toroidal contact of tyres. Friction at wheel and steering axes, non rigidity of materials, tyre compliance and tyre slip are neglected. Rider inputs are included, but set to zero in the analysis of self stability, and rider movement is neglected.

The characteristics of the bicycle model used by Meijaard et al are captured by 25 parameters. Parameters are defined with the bicycle upright on level ground with zero steer angle. Parameters are in relation to a coordinate system defined by the SAE 2001 convention, with the origin at the rear wheel ground contact point, x axis towards the front contact point, z axis down, and y axis to rider's right.

Meijaard et al describe the bicycle configuration in terms of parameters in
Table 1.

Parameter	*Symbol*	Units
Wheel base	ω	m
Trail	t	m
Head angle	α	degrees
gravity	g	N/kg
Forward speed	v	m/s
Rear wheel		
Radius	r_R	m
Mass	m_R	kg
Mass Moment of inertia	$(I_{Rxx},I_{Ryy},I_{Rzz})$	m
Rear Frame		
Position of centre of mass	(x_B,y_B,z_B)	m
Mass	m_B	kg
Mass moments of inertia	$\begin{bmatrix} I_{Bxx} & 0 & I_{Bxz} \\ 0 & I_{Byy} & 0 \\ I_{Bzx} & 0 & I_{Bzz} \end{bmatrix}$	kgm^2
Front Frame		
Position of centre of mass	(x_H,y_H,z_H)	m
Mass	m_H	kg
Mass moments of inertia	$\begin{bmatrix} I_{Hxx} & 0 & I_{Hxz} \\ 0 & I_{Hyy} & 0 \\ I_{Hzx} & 0 & I_{Hzz} \end{bmatrix}$	kgm^2
Front wheel		
Radius	r_F	m
Mass	m_F	kg
Mass Moment of inertia	$(I_{Fxx},I_{Fyy},I_{Fzz})$	m

Table 1: Bicycle Parameters

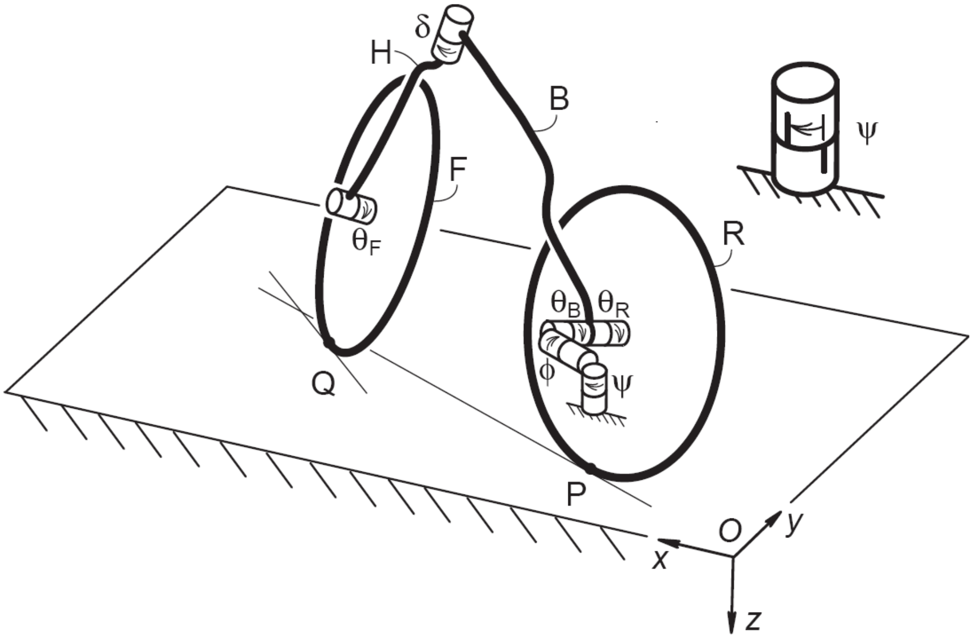

Figure 6 Configuration Space

From Figure 6 the bicycle's absolute position relative to a global reference frame xyz, with origin 0 may be defined. With rear wheel contact point at x_p, y_p known, global position of all other parts of the bicycle may be calculated from known values of rear frame yaw angle, ψ, rear frame lean angle, φ, and steer angle, δ. Other parameters necessary to define dynamics are front and rear wheel rotation, θ_R and $\theta_{F.}$ Rear frame pitch, θ_B is not a configuration variable as it may be calculated through a 3D trigonometric relation that keeps maintains front wheel ground contact. Other aspects of location such as locations such as wheel centre may be calculated from the seven dimensions of configuration space, x_p, y_p ψ, ϕ, δ, θ_R and $\theta_{F..}$

Meijaard et al, state that the model consists of three velocity degrees of freedom, once dynamic restrictions are placed on the 7 dimensional configuration space, such as tyre side slip not being allowed. Velocity space may be described by lean rate of the rear frame, steering rate and rotation rate of rear wheel, relative to rear frame.

In deriving linearized equations of motion, the first solution is the case of straight ahead, upright motion at any constant speed, with no forcing. This is the reference solution to the governing equations of motion. This first linearized equation of motion is reach through 2D mechanics in the xz-plane, giving

$$\left[r_R^2 m_T + I_{Ryy} + \left(r_R / r_F\right)^2 I_{Fyy}\right]\ddot{\theta}_R = T_{\theta_R}$$

For the remaining two velocity degrees of freedom, lean angle and steer angle, there are two coupled second order ordinary differential equations. The two equations can be combined as

$$\mathbf{M}\ddot{\mathbf{q}} + v\mathbf{C}_1\dot{\mathbf{q}} + \left[g\mathbf{K}_0 + v^2\mathbf{K}_2\right]\mathbf{q} = \mathbf{f}$$

Where $\mathbf{q} = \begin{bmatrix} \phi \\ \delta \end{bmatrix}$

$$\mathbf{f} = \begin{bmatrix} T_\phi \\ T_\delta \end{bmatrix}$$

The terms $\mathbf{M}$, $\mathbf{C}_1$, $\mathbf{K}_0$, and $\mathbf{K}_2$ are matrices of constants calculated from the design parameters of the bicycle.

$\mathbf{M}$ is a mass matrix, giving kinetic energy at zero forward speed, $\mathbf{C}_1$ act as a 'damping' matrix (although there is no true damping as the system is conservative), $\mathbf{K}_0$ and $\mathbf{K}_2$ are stiffness matrices, arising from gyroscopic and centrifugal effects. Calculation of these terms, as presented in Meijaard et al (2006), may be seen in Appendix 1.

2.2 Solutions to the linearized equations

When solved, the linearized equation gives a set of four eigenvalues, λ, for a given velocity. Meijaard et al (2006) present Figure 7 as the eigenvalues for their benchmark bicycle, over a range of velocities.

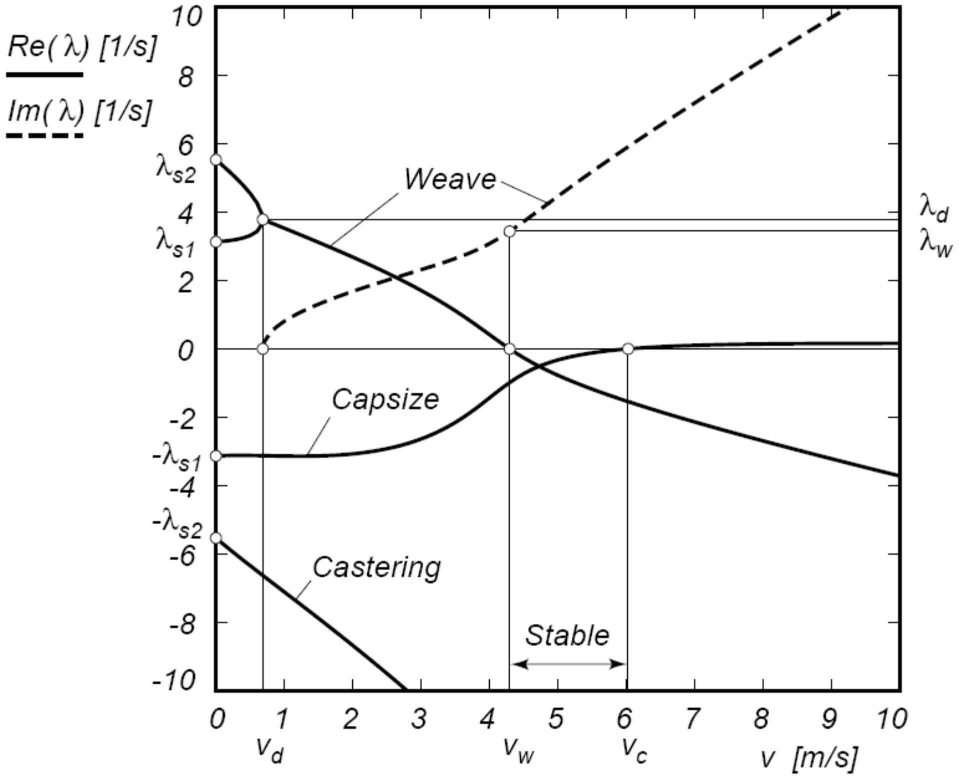

Figure 7 Stability Diagram

To extract useful information from a plot of eigenvalues of a system, an analysis based on bifurcations is necessary. Bifurcations of a system give rise to qualitative changes in dynamics. (Guckenheimer, 2007).

Hassard et al (1981) put forth that a system described by a Jacobian matrix, with a pair of complex conjugate eigenvalues, will be stable when eigenvalues, excluding their imaginary parts, are entirely negative. An instability will occur when the real part of an eigenvalue becomes positive. The appearance of this solution out of a state of equilibrium is known as a Hopf bifurcation. Hopf bifurcations are seen in the weave and capsize lines on either side of the stable region in Figure 7.

The other type of bifurcation seen in the eigenvalue plot is a saddle node bifurcation. The real part of the weave mode emanates from a pair of lines coming together in a saddle node bifurcation at sub-stable velocity. Hunt et al (2004), show that instability arises at the point a which a single line splits into two. Addition saddle node bifurcations in a system increase instability. The roll of saddle node bifurcations in stability analysis may be more easily understood when an analogy is drawn to the quadratic recurrence equation, which has the suggested use as a random number generator. A bifurcation diagram of iterations shows a series of progressively less stable regions, leading to chaos, as seen in Figure 8.

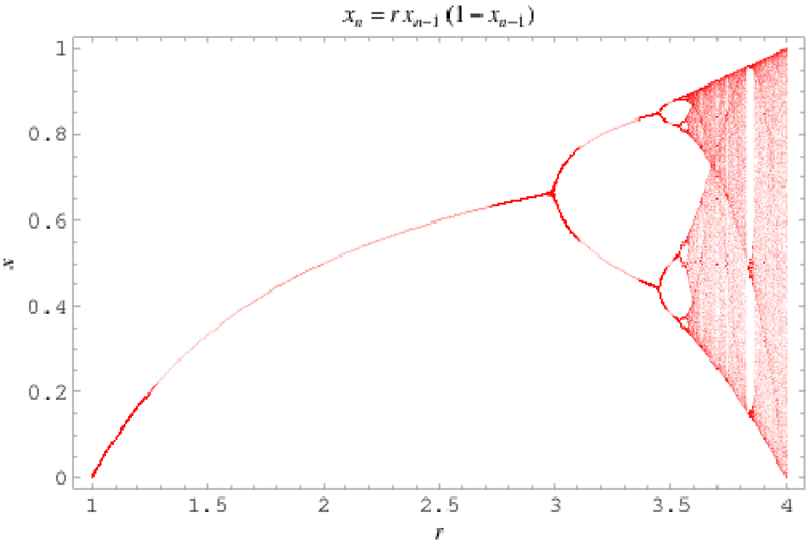

Figure 8 Quadratic Recurrence Bifurcation Diagram (Weinstein, *Wolfram Maths*)

Similar in appearance on an eigenvalue plot are pitchfork bifurcations, in which the original stable mode splits, to form three more modes. In a supercritical pitchfork bifurcation, two of the three formed modes will be will be stable, with one unstable mode. A subcritical pitchfork bifurcation results in two unstable and one stable mode.

2.3 Data Analysis

To extract useful information from experimental data points, parameters of a model must be found. In the context of bicycle dynamics, least squares fitting is most practical, due to its ability to fit a wide range of functions.

Least squares fitting works on the principal of reducing residual sum of squares. (Weisberg, 2005). As seen in Figure 9 , residuals are the vertical distance between the fitted line and the actual data points. Due to residuals being squared, the effect of outliers on fit is magnified. Method of data processing is discussed in more detail in Part 6.1.

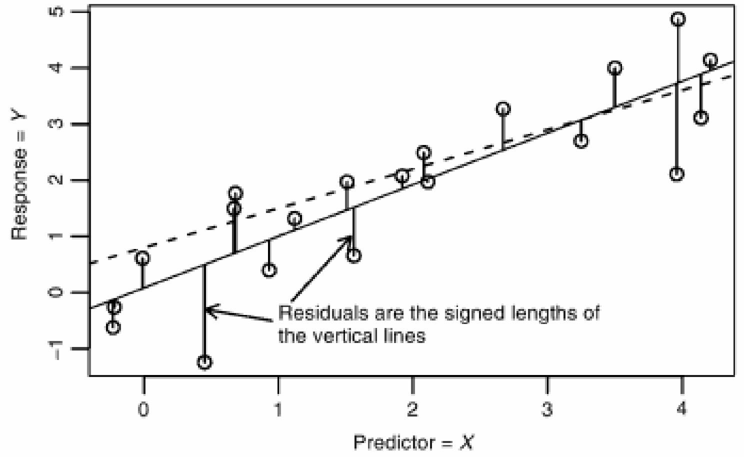

Figure 9 Residuals

3 Test Bicycle Design

To test the applicability of the linearized dynamics equation to a range of modern bicycle styles, a test bicycle with variable head tube angle was designed and built. The head angle was chosen as the variable factor due to its influence on handling being easily detected by a rider. The design aims to replicate steep head angle designs of modern track and road bikes, through commuter style bikes, to the slacker angles of downhill mountain bikes.

The variation of head tube angle affects other factors, such as wheel base, trail, centre of mass and moments of inertia. It is not possible to vary any individual factor, while holdings all others constant. As such, mathematical parameters of the bicycle must be recalculated for each head angle tested, before comparison to theoretical results.

Through the use of a single bicycle with variable head angle, uncontrolled variables are reduced. Masses are kept constant, wheel and tyre properties and most geometry is kept constant, as oppose to performing experiments using a number of different bikes. Also, mass properties of most parts will need only be calculated once, through one three dimensional model.

The design of the variable head angle mechanism focused on rigidity, fine adjustment, and ease of use. It was necessary to replicate the original configuration of the bike, as well as the head angles seen on other styles of bicycle.

Manufactured head angle is shown through a range of angle in Figure 10. Drawings are included in appendix.

Figure 10 Variable Head Angle

The head tube was cut from the frame, and a boxed section added, made from 2mm mild steel. Side plates were welded to the top and down tubes of the rear frame, and a pivot point drilled through the assembly. The head tube pivots on an 8mm bolt, and is restrained with a sliding aluminum linkage on the left side.

All manufacturing was carried out by the author, with a manual arc welder, angle grinder, electric drill and hand tools. Particular attention was paid to keeping the assembly square during welding and drilling, to ensure alignment of the bicycle.

Other modifications to the original bike were removal of crank assembly, saddle, brakes, handlebars, and cable stays on the frame. These components were not required in experimentation, and removal aided accurate computer modeling.

The front brake caliper was inverted to prevent the front wheel turning more than 90° and damaging the steering sensor.

Tyres had a smooth, grooved tread pattern for low rolling resistance and low vibration, compared to more aggressive tread patterns. Tyre pressure was maintained at 30psi. Wheel and steering head bearings were cleaned and greased, and hubs adjusted for minimal play before testing. Wheels were checked and found to be true.

To prevent damage to instrumentation, side wheels were added. This assembly was kept as light as possible to minimize changes to the bike's original mass properties. Small caster wheels were held approximately 750mm from each side of the bicycle, and 300mm above the ground. This restricted lean angles to around 22 degrees, and prevented damage to equipment under unstable conditions.

A rear rack was added to house the accelerometer, brackets added for the on board computer, and a restraint for the steering potentiometer, discussed in more detail in an upcoming section.

4 Modelling

To implement the linearized equation of motion, characteristics of the bicycle must be known. Due to the complex form of the bicycle, calculating centres of mass and moments of inertia for every tested configuration was not practical. As such, the test bicycle was measured, and modeled accurately in three dimensions using ProEngineer, with the inclusion of a variable head tube angle. An output of mass properties was then able to be produced for each wheel, front frame, and rear frame with instruments attached.

Measurements were made with Sontax digital vernier calipers, tape measure and large ruler. The calipers were accurate to 0.01mm, and were used for tube diameter and material thicknesses. Larger dimensions were taken to the nearest millimeter. Angular measurements were taken with a Craftright digital angle gauge. The gauge had a resolution of 0.1 degrees and was tested for accuracy by inversion on various slopes.

Figure 11: Craftright Digital Angle Gauge.

Figure 12: Instrumented Bicycle

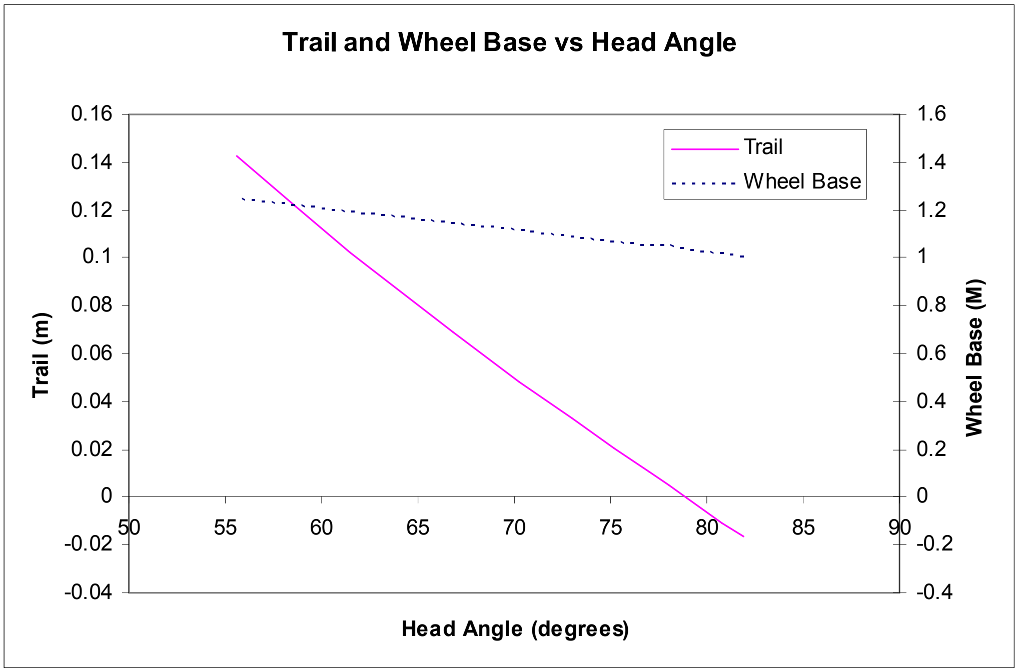

Figure 13: Variation of Trail and Wheelbase

Figure 14: Complete 3D Model

The model was developed as a mechanism, with constraints as follows. The origin of the coordinate system was held at the rear wheel ground contact point, with the system oriented as seen in the Meijaard (2006) bicycle model. The head angle was made variable by the use of a pin constraint at the hinge point, between the modified head tube and rear frame. The ground contact point of the front wheel was set to allow movement along the x axis, governed by head angle. To maintain ground contact at front and rear wheels, front frame and rear frame were allowed to translate along their own plane of symmetry, the x-z plane. Pin joints at the front and rear axle locations completed the model.

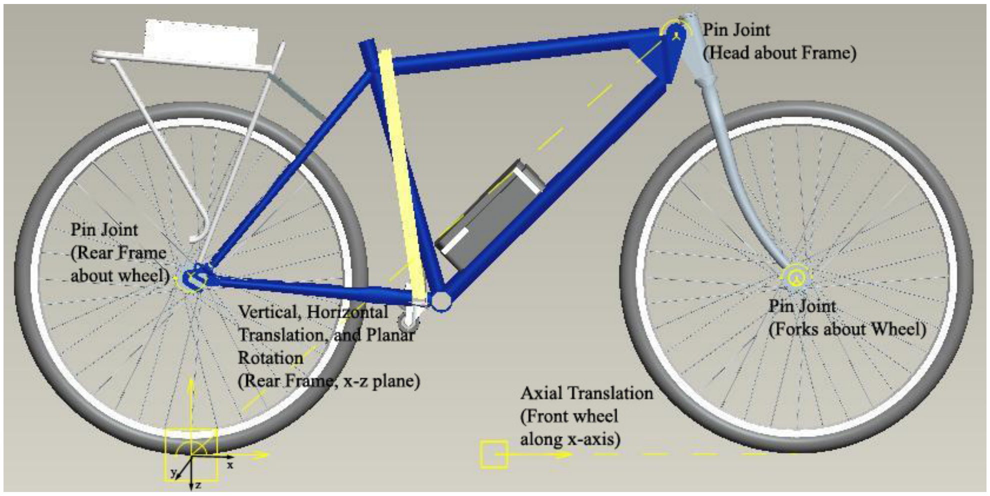

Figure 15 Constraint System

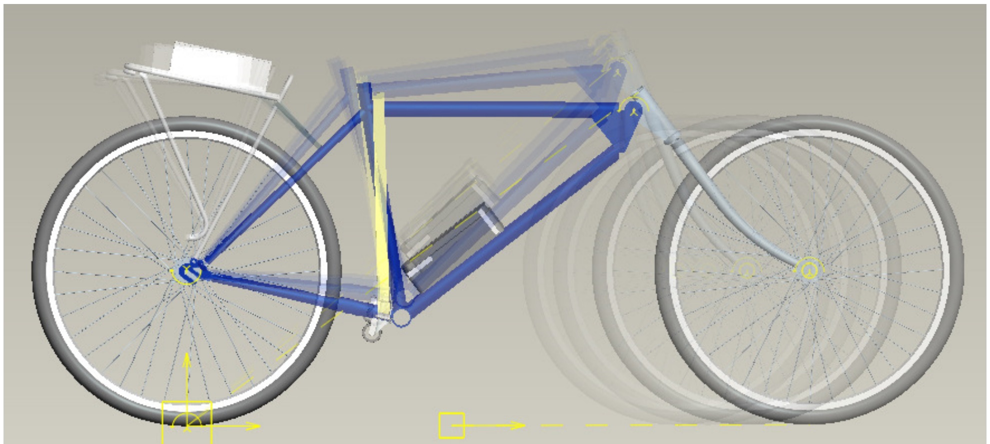

Figure 16: Head Angle Variation

To verify Pro Engineer mass property outputs, calculated values were compared to physically measured units. The bicycle was disassembled and parts were weighed on a scale with 5g accuracy, and compared to Pro Engineer model mass output values. Parts with unknown density, or hidden internal dimensions were adjusted in the 3D model to concur with measured masses.

Response of trail and wheelbase to changes in head angle was investigated, and shown in Figure 13.

4.1 Pro Engineer Mass Properties

Pro Engineer outputs all necessary mass properties for stability analysis of the modeled bicycle. With the rear wheel ground contact point positioned at the origin, useful properties will be produced.

From the mass properties output file, required parameters are mass, centre of gravity, inertia tensor with respect to rear wheel ground contact point and with respect to centre of gravity, principal moments of inertia and a rotation matrix, defining orientation of principal axes relative to global coordinate system.

Due to symmetry in the model, the rotation matrix takes the form,

$$R(\gamma) = \begin{bmatrix} \cos\gamma & \sin\gamma & 0 \\ -\sin\gamma & \cos\gamma & 0 \\ 0 & 0 & 1 \end{bmatrix},$$

with γ being the angle of rotation about the z axis. Radii of gyration is produced, as are centres of mass of each part in an assembly.

To gather mass properties of individual components, relative to rear wheel contact point, unwanted components are suppressed, and a mass property analysis is run.

5 Bicycle Instrumentation

To define the movement of the bicycle, the three velocity degrees of freedom are measured, that is steer angle, rear frame lean angle, and rear wheel rotation. These parameters are measured by sensors, sending signals to a SoundBook. The Sinus SoundBook Octav is a modified notebook computer, most commonly used for tasks in acoustics and vibration analysis. The SoundBook has 8 acoustic inputs, with a sampling frequency of 51.2kHz. The SoundBook is based on the Panasonic CF19 laptop, designed as a dust, moisture and vibration proof computer. The system offers touchscreen operation, which is convenient when the computer is mounted on the bicycle.

Figure 17: Sinus SoundBook (mikrofonen.se)

Steering angle was transmitted using a 500kΩ linear potentiometer, wired in a voltage divider arrangement with a 9V battery.

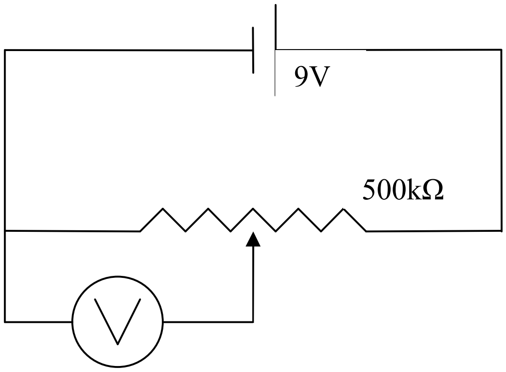

Figure 18: Voltage divider arrangement, for steering angle, with SoundBook used as voltmeter.

The body of the potentiometer had the same diameter as the steerer tube of the forks, and was held in place with a hose clamp. The stem of the potentiometer was fixed relative to the head tube with a custom bracket. The most important factor in mounting was the elimination of movement between the potentiometer and the parts it referenced.

Figure 19: Steering angle potentiometer, and restraint.

The output was measured with the SoundBook through a range of known angles, allowing a calibration factor to be determined. Output was recorded directed by the SoundBook during experimentation.

Rear wheel speed was recorded through a magnetic reed switch mounted on the frame, and a single pole magnet mounted on the wheel spokes. The magnet closed the reed switch once every rotation, sending a momentary voltage from a 9V battery to the SoundBook.

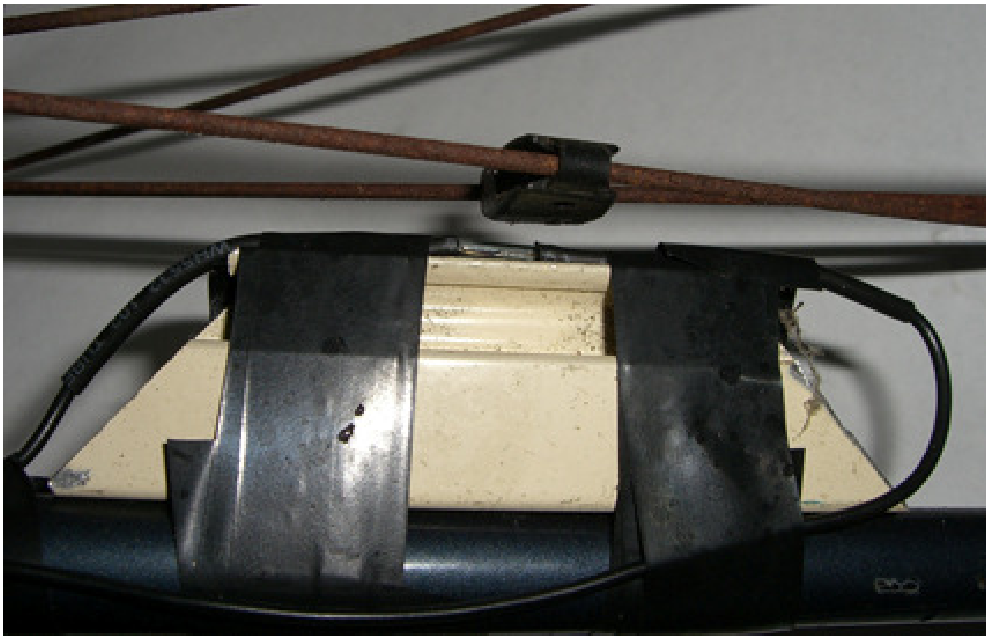

Figure 20: Rear Wheel Speedometer

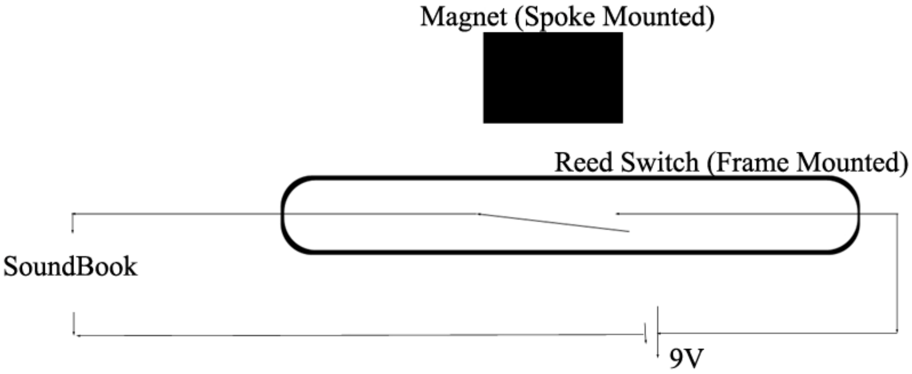

Figure 21: Speedometer Diagram

The bike was also fitted with a standard wireless cycle computer (Figure 22), reading velocity from the front wheel, to allow velocity monitoring by the launcher during testing.

Figure 22: Cateye Wireless Speedometer

Ideally, angular rates of the rear frame would be measured with angular rate sensors or gyroscopes. Under the constraints of an undergraduate thesis, these were not available. As such, angular rates were calculated from measured acceleration values. A triaxial accelerometer (Figure 23) was mounted on a rack directly above the ground contact point of the rear wheel. Assuming no lateral motion of the rear tyre relative to the ground, lean may be calculated from acceleration data.

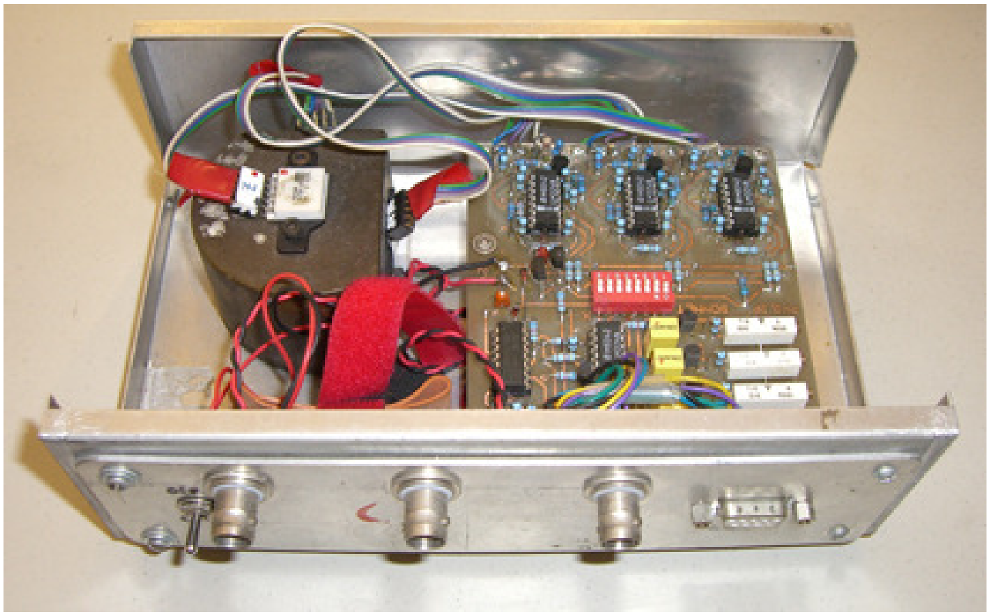

Figure 23: Accelerometer

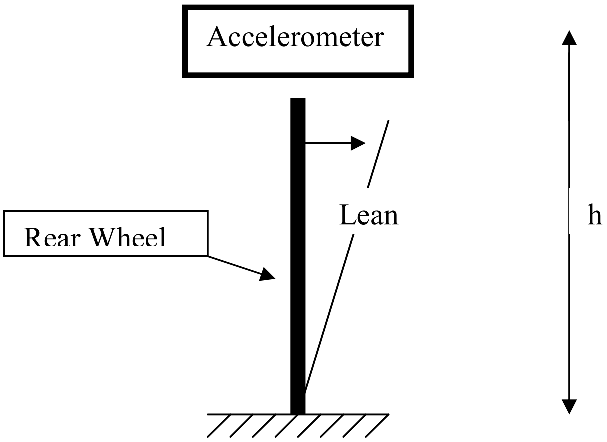

Figure 24: Lean of Rear Frame

With reference to Figure 24, angular rate of rear frame is simply equal to acceleration multiplied by elevation (h), of accelerometer.

Instrument Calibration

A calibration factor was found, to convert the steering angle potentiometer's voltage output to radians. With the bicycle's frame held horizontal, the steering angle was able to be precisely measured using the Craftright digital angle gauge.

Voltage was plotted against steering angle, and the calibration equation was found to be $\delta = 0.5807V - 0.0623$.

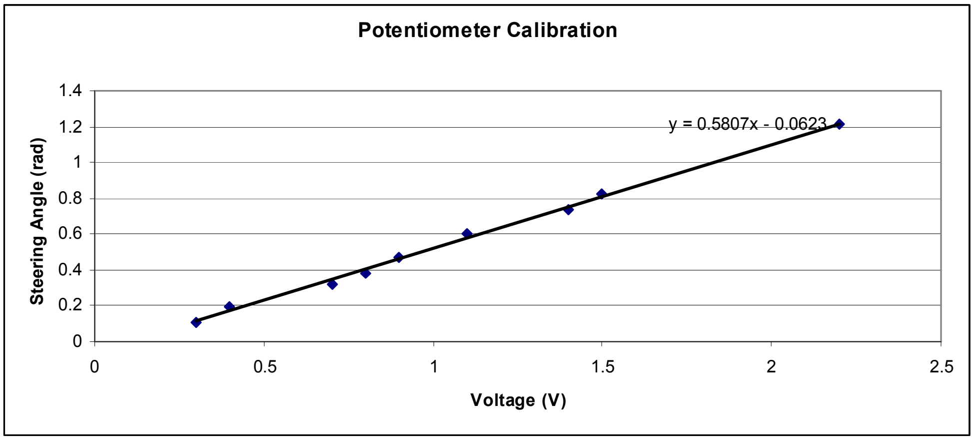

Figure 25: Potentiometer Calibration

Rear wheel speedometer output is a digital signal, corresponding to period of revolutions of the rear wheel (T). Rear wheel rotation rate may be calculated as

$$\dot{\theta}_R = 2\pi / T$$

And velocity calculated as

$$V = Diameter_R / T$$

Calibration of the accelerometer was done through inversion for each axis. With the axis to be held vertically, the output was measured, and then the accelerometer inverted, to change resting acceleration by 2g, before measuring voltage again. The results are as follows in Table 2, including offset, equal to resting voltage with y-axis vertical.

Axis	Sensitivity (V/m/s^2)	Offset (V)
x	0.339	6.73
y	0.054	4.8
z	0.04638	5.1

Table 2 Accelerometer Calibration

6 Experimental Procedure

The experiments aimed to determine stable speeds of the bicycle, through a variation of head tube angles. Motion of the bicycle was captured by on board instrumentation, showing range of speeds for weave, capsize and caster.

Tests were conducted on outdoor netball courts, with a smooth asphalt surface.

The launch speed was limited by how fast the launcher could run, i.e. just above 20km/h.

Two methods were used to determine the stable speed range for a range of head angles.

Firstly, the bicycle's motion was observed, giving a subjective indication of stability. At each set head tube angle, the bicycle was accelerated to test speed by hand and released. Observations were made, as to whether the bicycle fell immediately, remained upright, or capsized. At speeds where the bicycle remained stable after being released, the launcher ran beside the bike to note the speed at which the bike became unstable.

As part of subjective observations, disturbances were introduced to observe whether or not the bicycle recovered stability. Through gradually changing the velocity at which the disturbance was introduced in each test, an approximation of self stable velocities could be made.

Speedometer readings and points of instability were verified through observation of SoundBook recording after testing.

The second method used numerical analysis of the bicycle's motion to find eigenvalues of the dynamic equation, in turn allowing a plot to be produced, showing stable speed range for each head angle. For each tested head angle, the bicycle was released, and a disturbance introduced. The disturbance forced the bicycle to into a lean, followed by weave before regain of stability, or loss of stability. The analysis produces one set of eigenvalues, corresponding to the range of velocities over which they were calculated, that is, the range of speeds after disturbance at which the bicycle exhibited weave. In order to produce a meaningful plot from measured eigenvalues, results were collected for 10 velocities at each head angle, with 11 head angles tested.

The motion analysis process is discussed further in an upcoming section.

6.1 Data Processing

To calculate a stable speed range for each tested head angle, eigenvalues had to be extracted from data recorded by the SoundBook. All data processing was carried out with MatLab.

For all sensors, the SoundBook records a one dimensional data signal, with a known sample frequency of 51200Hz. This vector was multiplied by the calibration constant for the respective sensor to convert the data from a voltage to the required unit.

In order to plot the data, a time vector had to be created, of the same length as the data signal. The interval between each time point was the period of the sampled data. For example, a sample of 1000000 data points at 51200Hz, requires a time signal 19.53 seconds long, with 1/51200 second intervals.

The initial data showed considerable noise in all cases, so a 1001 point moving average smoothing method was applied. From this, areas of the test run exhibiting weave motion were visible. These areas were used in curve fitting.

As the motion is an exponentially decreasing oscillation, the data was fitted to the general equation,

$$y = e^{d(x)}\ (c_2 \cos(\omega x) + c_3 \sin(\omega x)) + c_1$$

Matlab's *curvefit* interface was used. A least squares method was used, and to reduce the number of evaluations required, limits were set on constants. The most easily calculated constant was the frequency,

$$\omega = \frac{2\pi}{P}$$

Where p is the period between peaks in oscillation.

Rough limits could be set on constant c_1, through observation of overall offset in the y axis.

7 Results

7.1 Experimental Observations

Through observation, different head angles displayed different stable velocity ranges. It was seen that the bike's minimum stable speed was lower for steeper head angles, to a point. In all cases, it appeared that maximum stable speed was faster than maximum achievable launch speed.

Most significant observations were as follows.

At head angles greater than 66.8°, the bicycle did not correct instabilities, within the maximum achievable launch speed. The bike slowly fell to one side, whilst entering a tightening spiral.

Self stability was observed at 66.8°, at speeds above 5.7m/s. In response to lean, the bike would weave, and return to an upright position.

As the head angle was reduced, stability was observed at progressively lower speeds. At 62.6°, stability was observed at as low as 3.8m/s. From this point, minimum stable speed seemed to increase, with a 58.6° head angle exhibiting self stability above 4.1 m/s, and a 55.6° head angle stable above 4.2m/s.

With a head angle lower than this the bicycle became difficult to launch, and did not appear to be showing self stability.

7.2 Calculated Stability Ranges

Stable speed ranges were predicted using the linearized dynamics equations, with mass properties from the Pro Engineer model. Matlab was used to calculate and plot real and imaginary parts of the eigenvalues for each tested head angle.

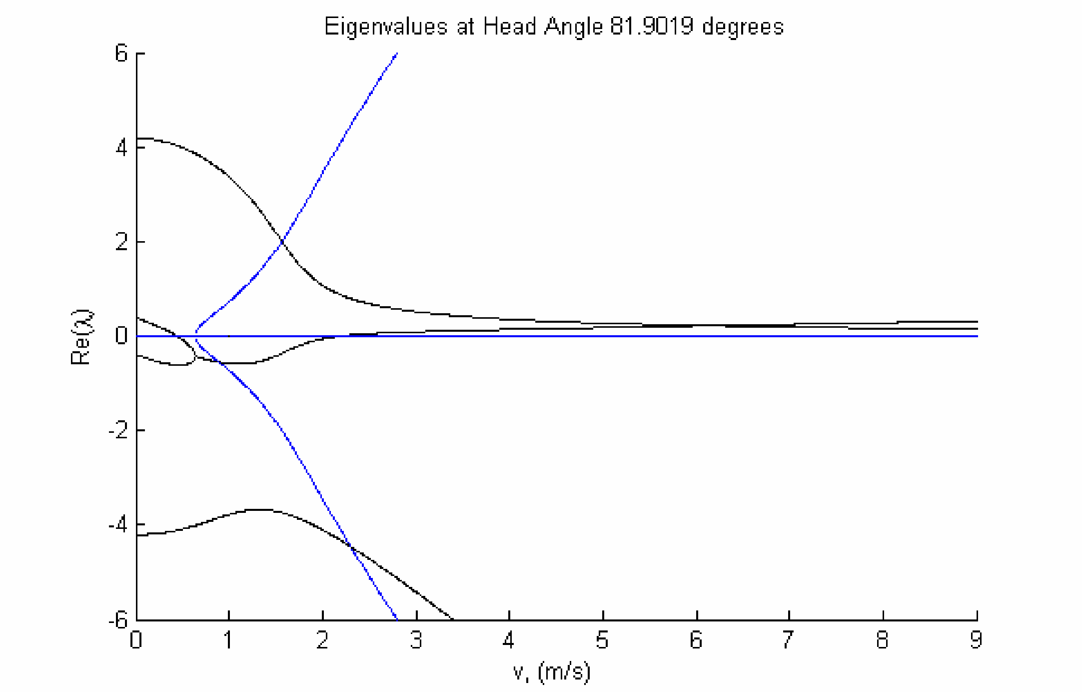

Figure 26: Eigenvalue Plot, head angle 81.9°. Black lines represent real parts of eigenvalues, while blue represents imaginary parts.

At 81.9°, there is no stable velocity region. The real part of the weave move eigenvalue does not become negative within the tested range, and more significantly, not before capsize mode eigenvalue turns positive. The capsize mode begins from a saddle node bifurcation, turning more negative before a reversal in gradient and turning positive.

The castering mode grows, before becoming progressively more negative.

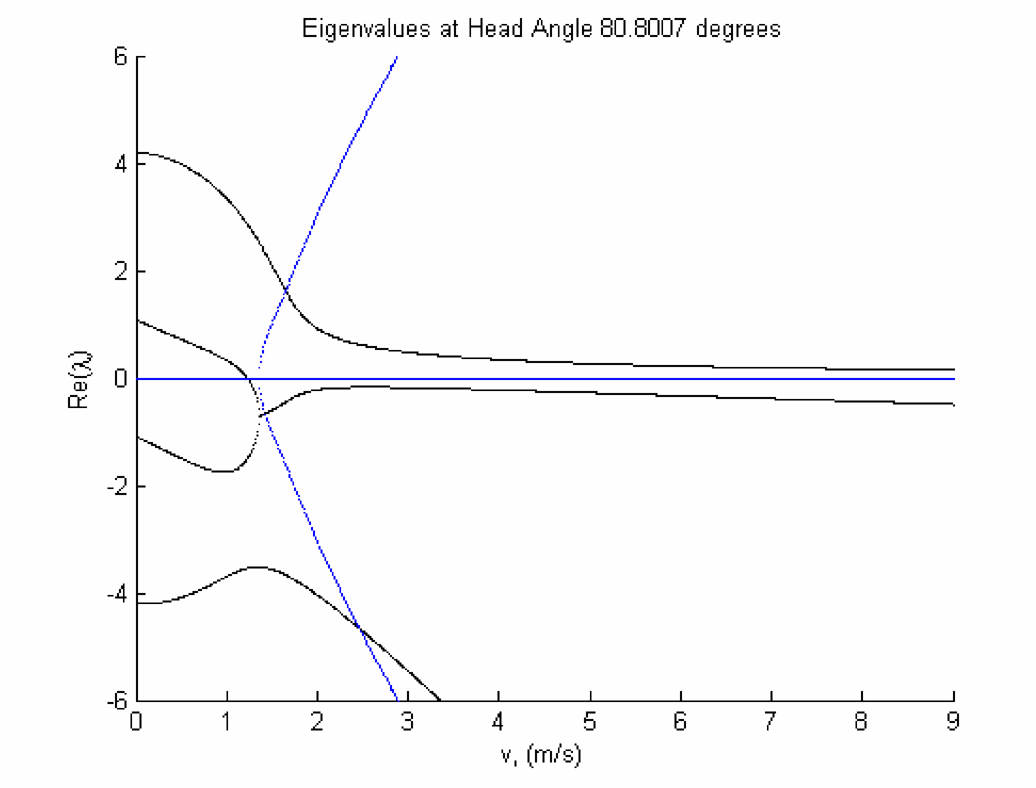

Figure 27: Eigenvalue Plot, head angle 80.8°.

Again no stability is observed. In this case the capsize mode arises from bifurcation, in addition to never crossing the x-axis. The area before bifurcation of the capsize mode line has expanded, in comparison to Figure 26.

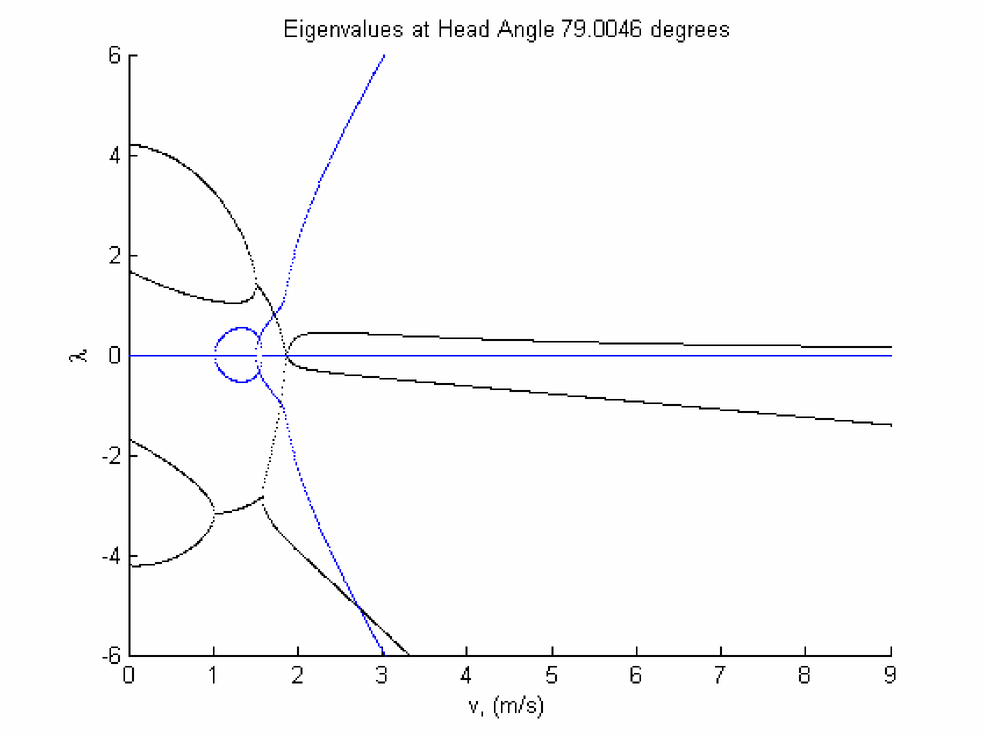

Figure 28: Eigenvalue Plot, head angle 79.0°.

At a head angle of 79°, there is no stable region. It can be seen that the saddle node bifurcation of Figure 27 is no longer present, and two new bifurcations have appeared. A second set of imaginary parts is seen, which is absent at higher head angles. This ends in a saddle node, at the velocity of capsize and caster mode creation.

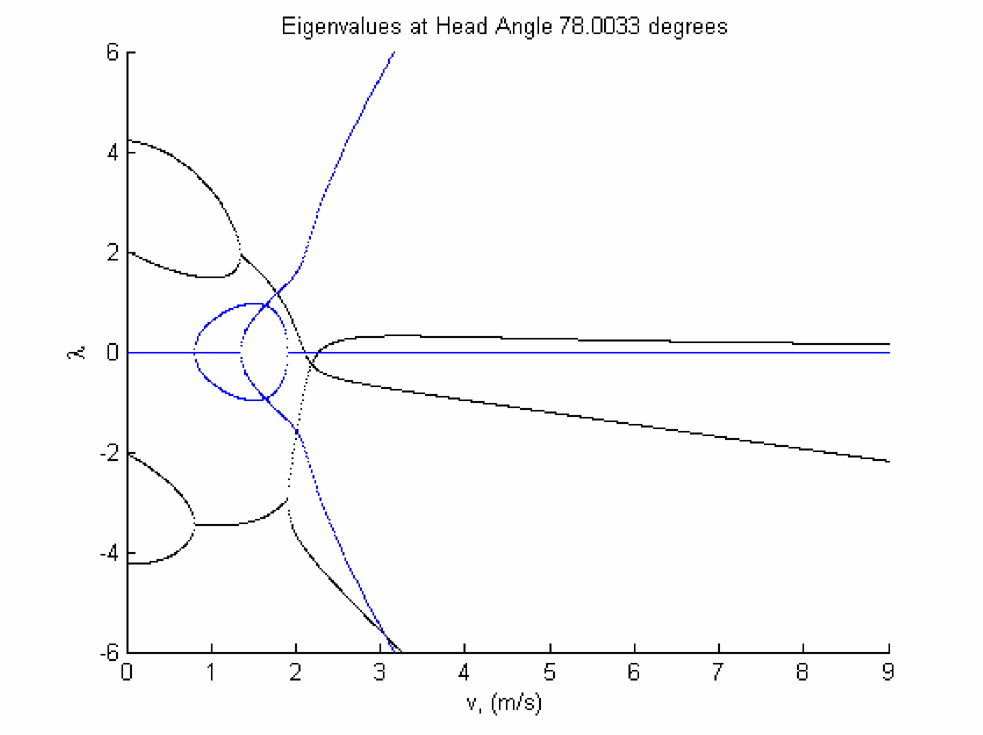

Figure 29: Eigenvalue Plot, head angle 78.0°.

This exhibits a region suggesting stability, marginally above 2m/s, but the capsize mode results from a saddle node bifurcation. Again the capsize mode arises from bifurcation, rather than being a separate mode from zero velocity. In general, features of the graph such as intercepts are occurring at a higher velocity than seen at steeper head angles.

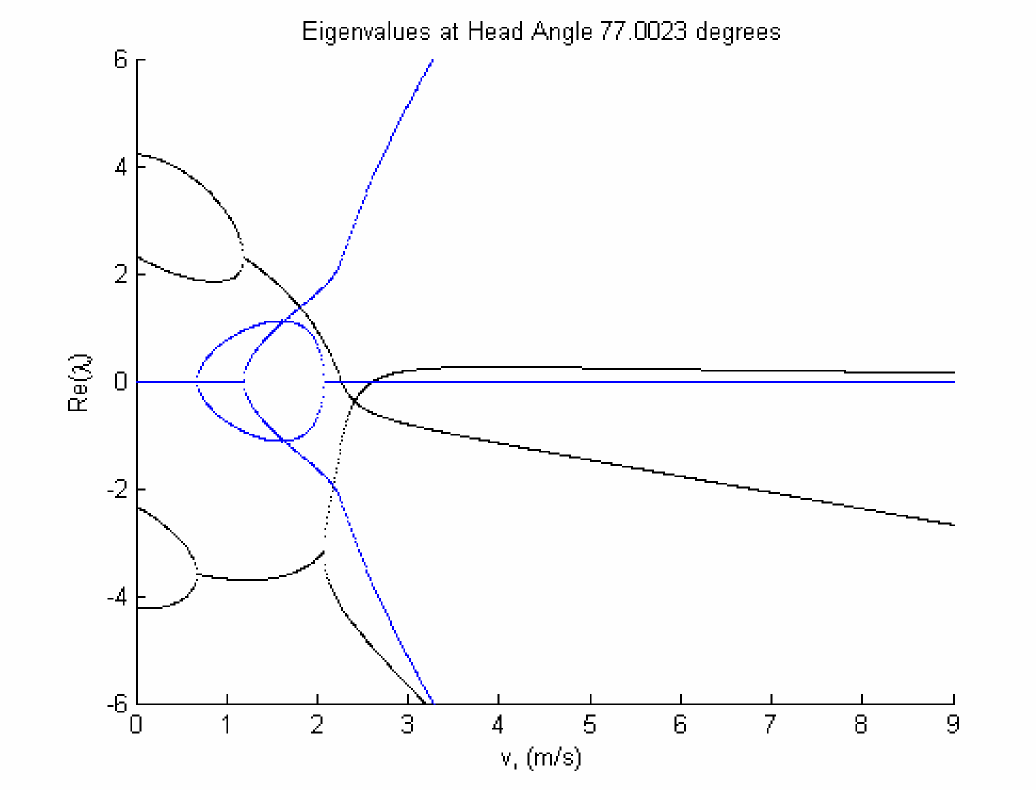

Figure 30: Eigenvalue Plot, head angle 77.0°.

At 77° the trends seen previously continue, and the region of negative real roots occurs over a larger range of velocities. It can be seen that the real part of the weave mode is decreasing with a steeper gradient than seen previously.

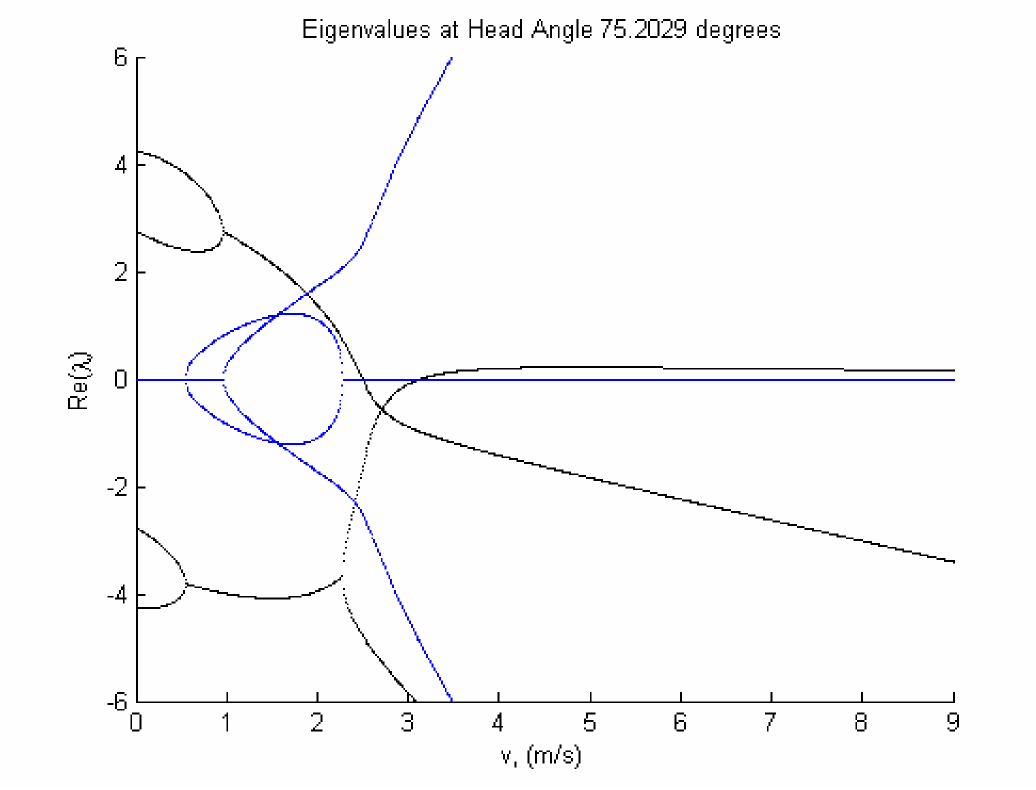

Figure 31: Eigenvalue Plot, head angle 75.2°.

Results for 75.2° take similar form to 77°, with the seemingly stable region larger, and with a higher minimum stable velocity.

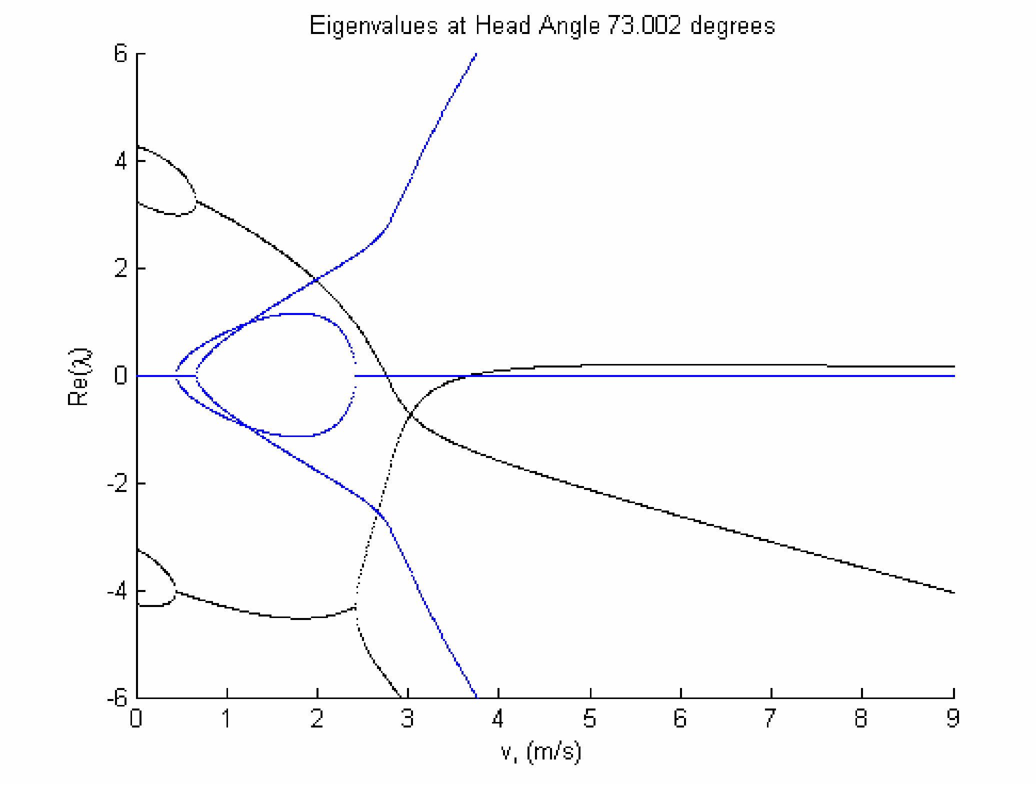

Figure 32: Eigenvalue Plot, head angle 73.0°.

A trend of larger and higher stable speed range continues, as does the presence of a saddle node bifurcation forming the caster and capsize modes.

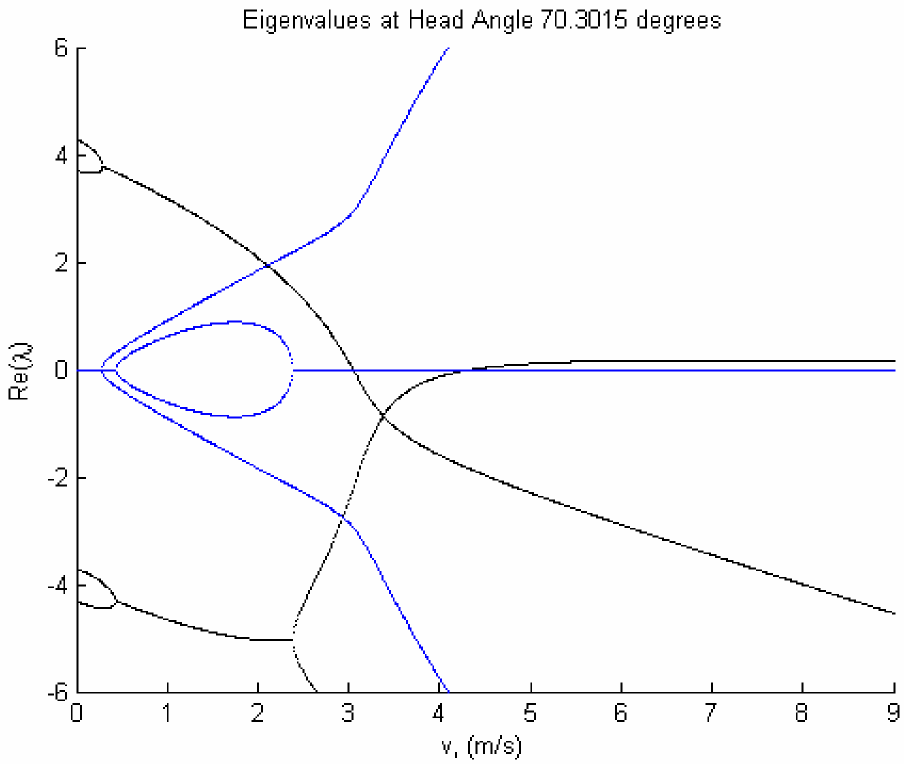

Figure 33: Eigenvalue Plot, head angle 70.3°.

At 70.3°, the areas before bifurcation in the real modes have moved noticeably closer to zero velocity. The region where caster and capsize are merged is larger, as is apparent stable speed region.

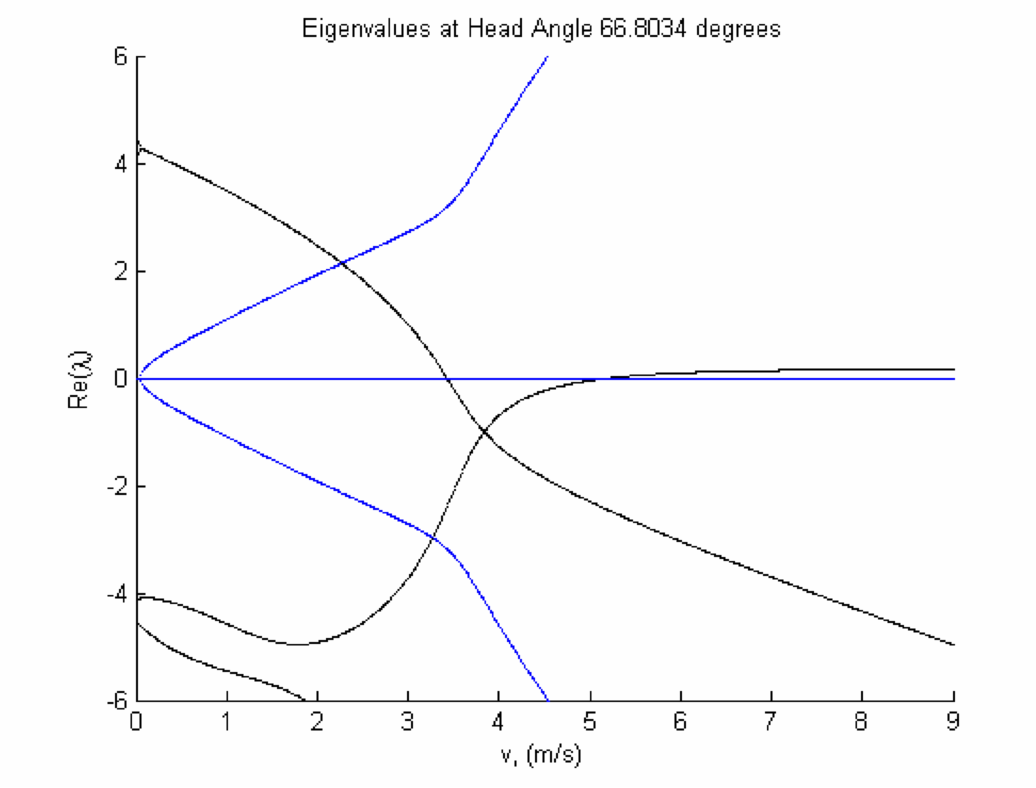

Figure 34: Eigenvalue Plot, head angle 66.8°.

At a head angle of 66.8°, separate capsize and caster modes exist from zero velocity. As such, the addition set of imaginary parts are no longer present. At true stable speed range is now seen, and is larger than apparent stable speed region of previous graphs. Furthermore, the minimum stable speed continues to increase. At this head angle, results take the same form as those for the benchmarked stable bicycle used by Meijaard et al (2006). The minimum stable speed is 3.425m/s, and the maximum is 5.225m/s.

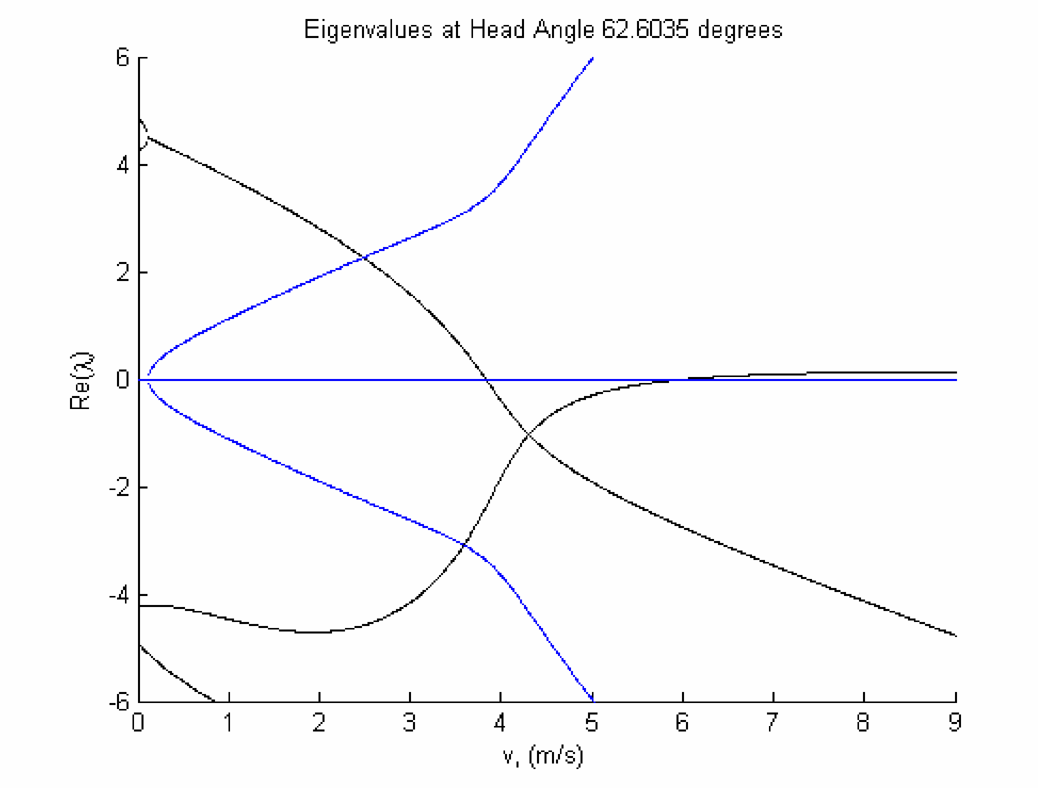

Figure 35: Eigenvalue Plot, head angle 62.6°.

Capsize and caster modes remain separate from zero velocity, and stable speed range continues to increase. At this angle, minimum stable speed is 3.83m/s and maximum is 6.06m/s. It is also noted that the values of the caster mode are dropping as head angle decreases.

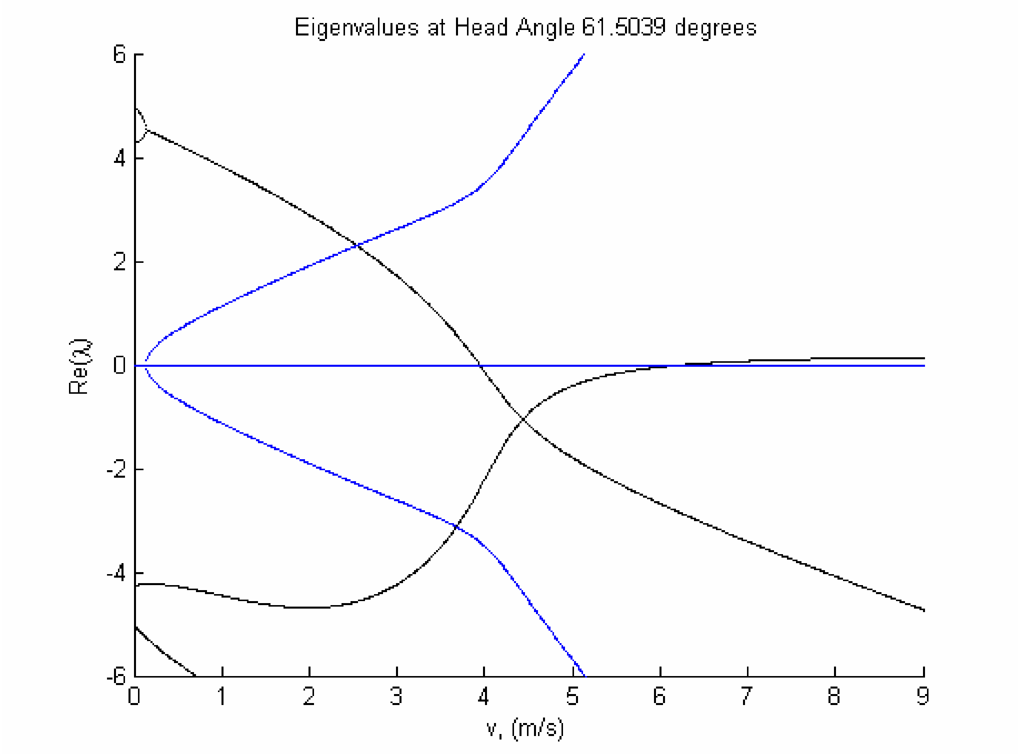

Figure 36: Eigenvalue Plot, head angle 61.5°.

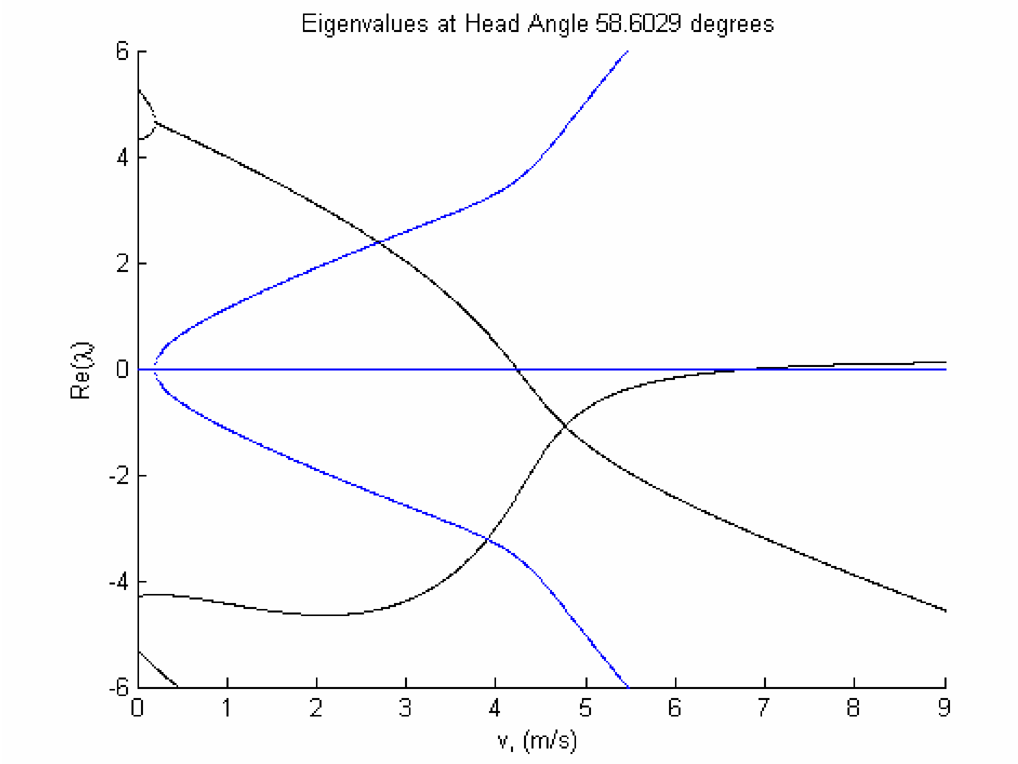

Figure 37: Eigenvalue Plot, head angle 58.6°.

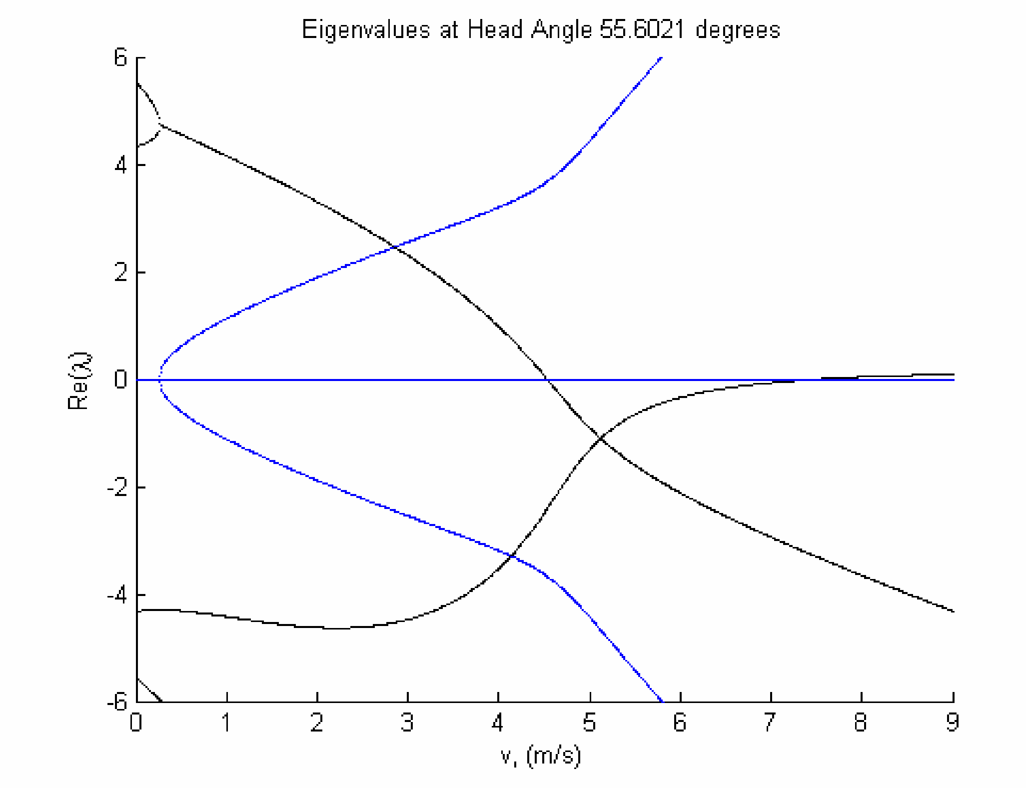

Figure 38: Eigenvalue Plot, head angle 55.6°.

Through head angles 61.5°, 58.6°, and 55.6°, the stable speed range increase in magnitude and range. Caster mode values decrease. Since the 66.8°, the angle at which separate caster and capsize modes started to appear, the double root in the weave mode line has occurred at a progressively higher velocity. Subsequently, the pair of imaginary roots also begin at higher velocities.

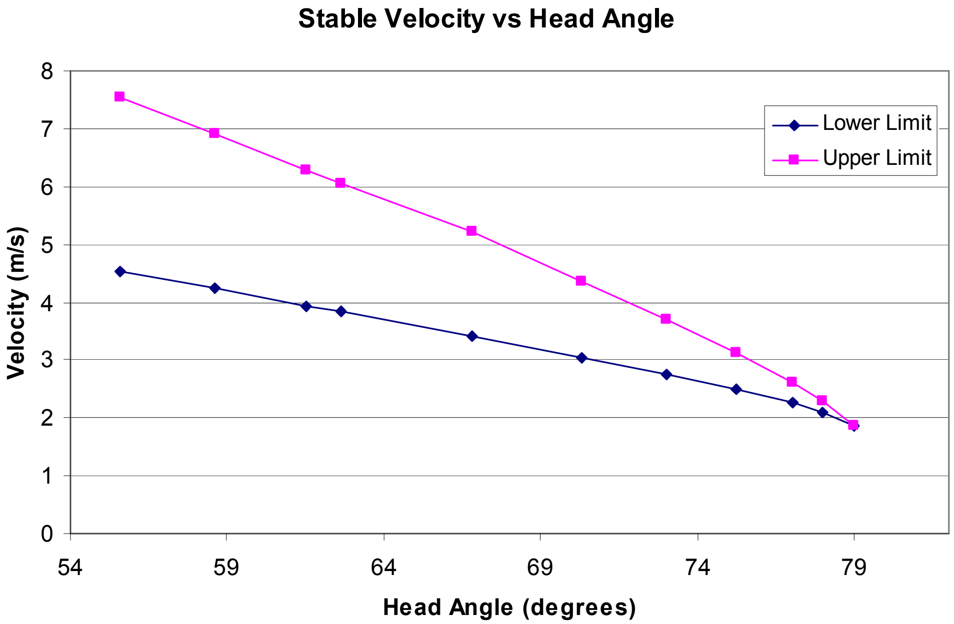

Figure 39: Stable Velocity vs Head Angle

The response of stability to variations in head angle is seen in Figure 39. In general, as the head angle gets steeper, the range of stable speeds becomes narrower and lower.

7.3 Experimental Results

For each test run, data was recorded at 51200Hz for velocity, steering angle, and acceleration in the x and y directions for the rear frame above the rear ground contact point. A typical set of results is shown in Figure 40. This set of data was recorded with a head angle of 80.8°. A lateral disturbance was introduced at 2.8 seconds, seen as a negative peak in Figure 40. This leads to a visible oscillation, before returning to rest, also seen in the steer angle, Figure 41.

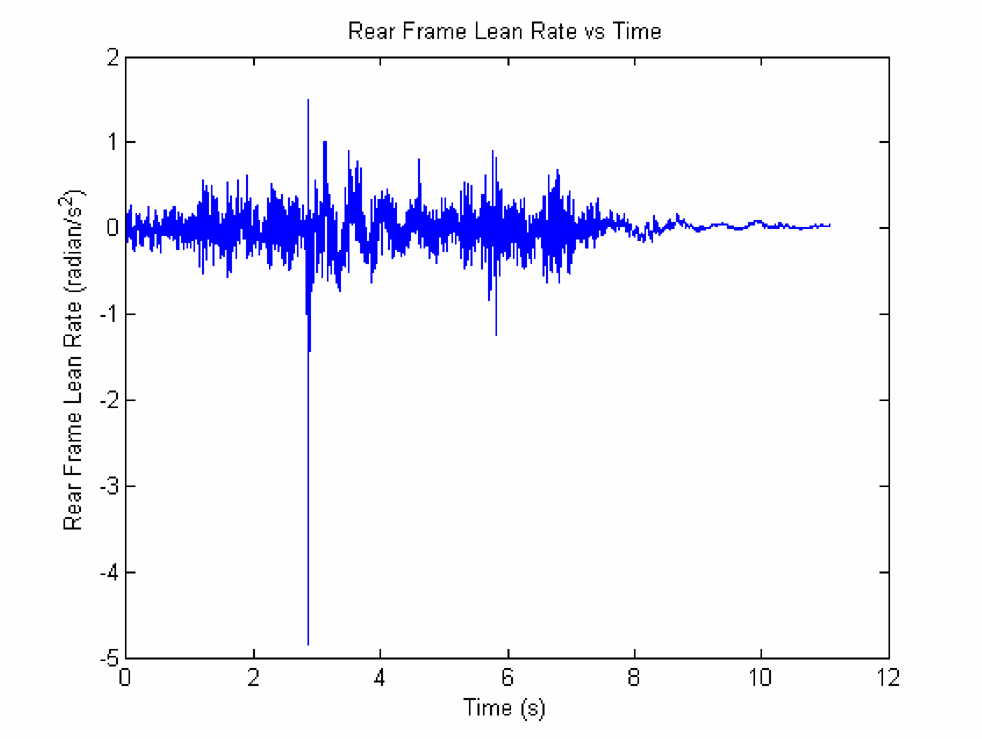

Figure 40: Rear frame lean rate, for head angle 80.8°.

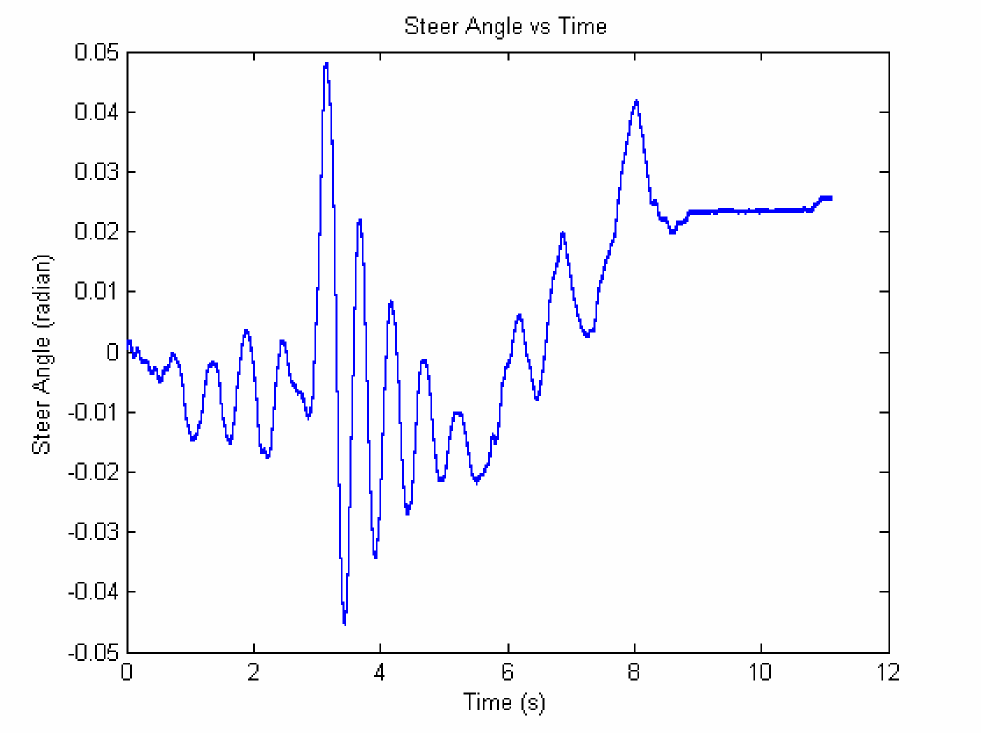

Figure 41: Steer angle output, for head angle 80.8°.

Velocity is recorded as a pulse signal, shown in Figure 42. This is also displayed in Figure 43, as a calculated velocity, in m/s.

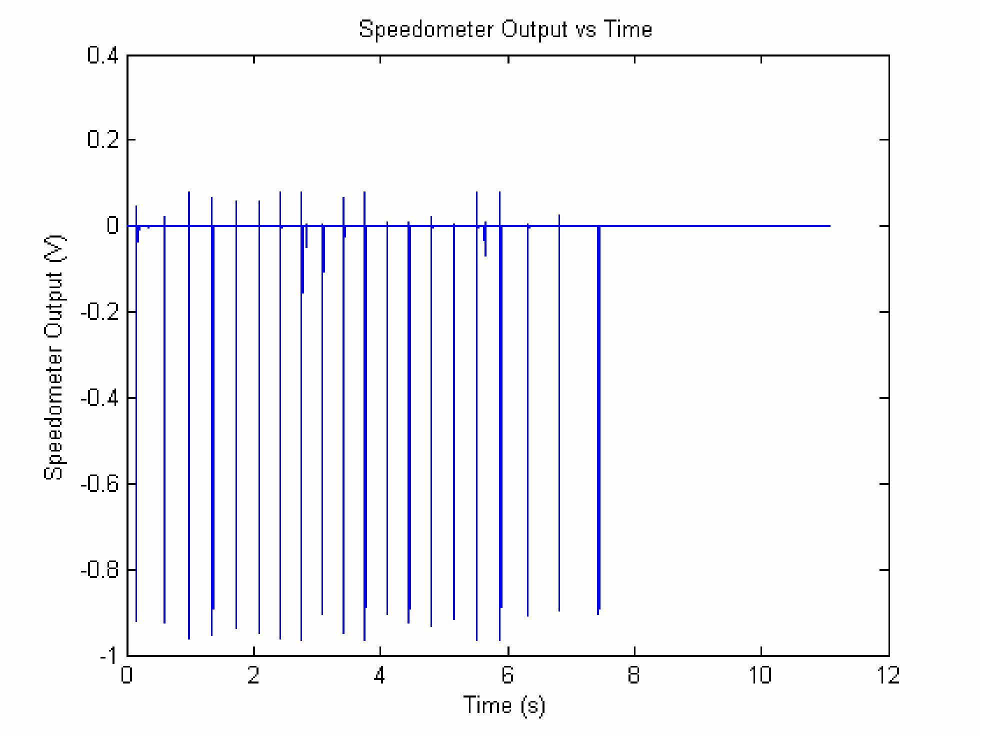

Figure 42: Rear Wheel Speedometer Output, head angle 80.8°.

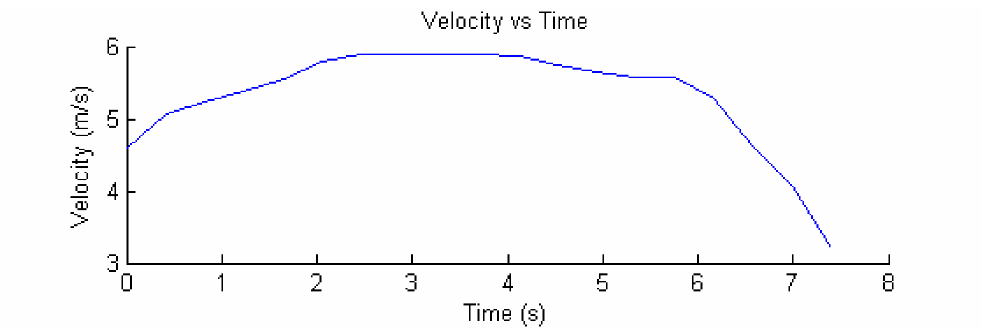

Figure 43: Velocity vs time, head angle 80.8°.

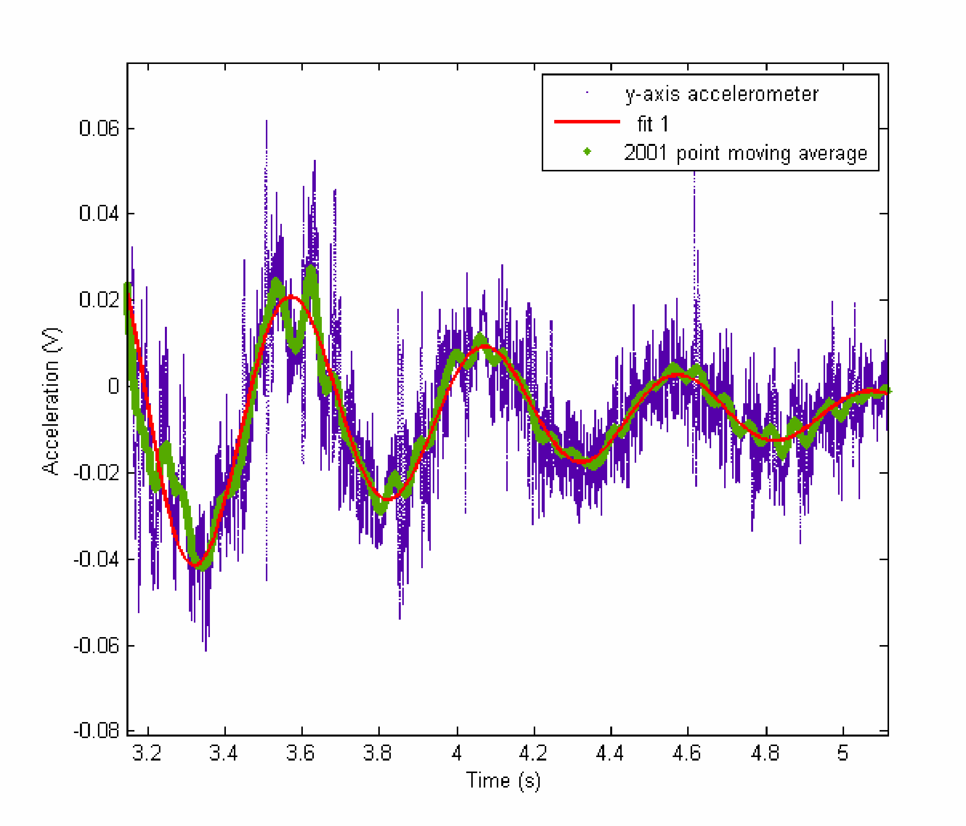

Figure 44: Lean rate curve fitting, for head angle 80.8°.

Figure 44 shows a selection of lean rate data directly after a momentary lateral disturbance was applied to the bicycle. The data considered for curve fitting is between 3.2 and 5 seconds, where the velocity varies from 5.93m/s to 5.57m/s.

In fitting a curve to the data, the general equation was:

$$f(x) = e^{(\delta . x)}(b\cos(\omega x) + d\sin(\omega x)) + e$$

Giving weave frequency $\omega = Im(\lambda_{\text{weave}})$ and the damping $\delta = \mathrm{Re}(\lambda_{\text{weave}})$.

Using nonlinear Least Squares fitting, in MatLab's curve fitting tool, the curve's equation was found to be

$$f(x) = e^{(-1.126 \times x)}(0.8475\cos(12.56x) + 1.242\sin(12.56x)) - 0.00603$$

This gives an eigenvalue for the weave mode of -1.126 + 12.56i, over the velocity range 5.57m/s to 5.93m/s.

Repeating this process for other runs at the same head angle gives a series of eigenvalues, plotted in Figure 45.

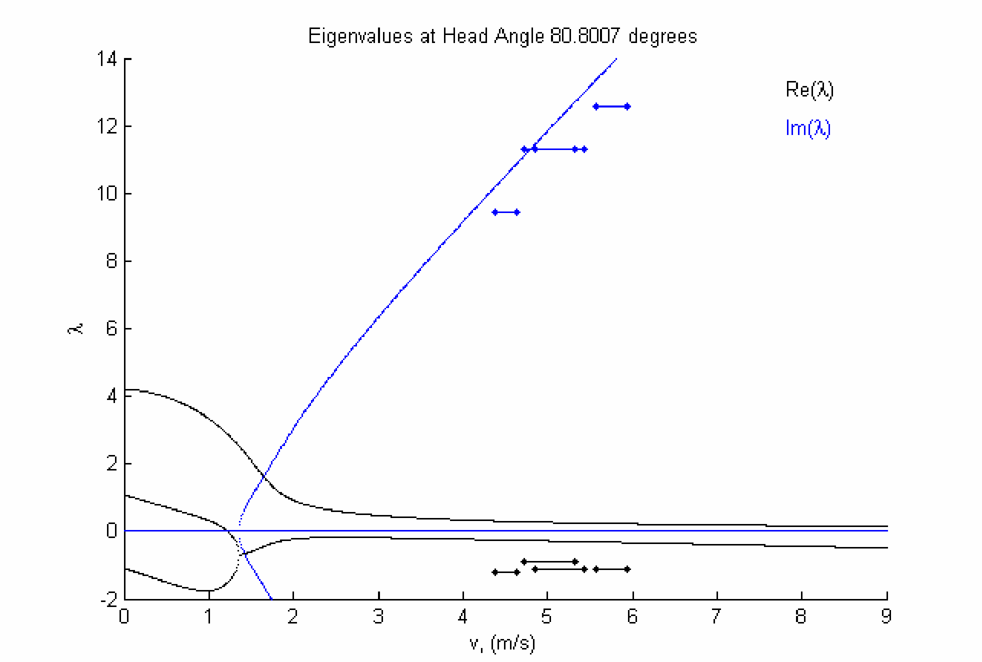

Figure 45: Experimental eigenvalues, head angle 80.8°. Eigenvalues are calculated over varying velocities, shown as bars in the plot. Values predicted by the linearized equation are plotted as continuous lines, for comparison.

The results gained for a head angle of 80.8°, show some relation to the weave mode lines (see Figure 7). Imaginary parts show a trend as would be expected from the linearized equations. Real parts of measured eigenvalues are negative, whereas the predicted weave line does not become negative at this head angle.

Due to lack of stability, oscillatory behavior was only able to be invoked at relatively high velocity, during capsize. Increased accelerometer noise, and relatively small angular variation in steering oscillations led to lack of useful data.

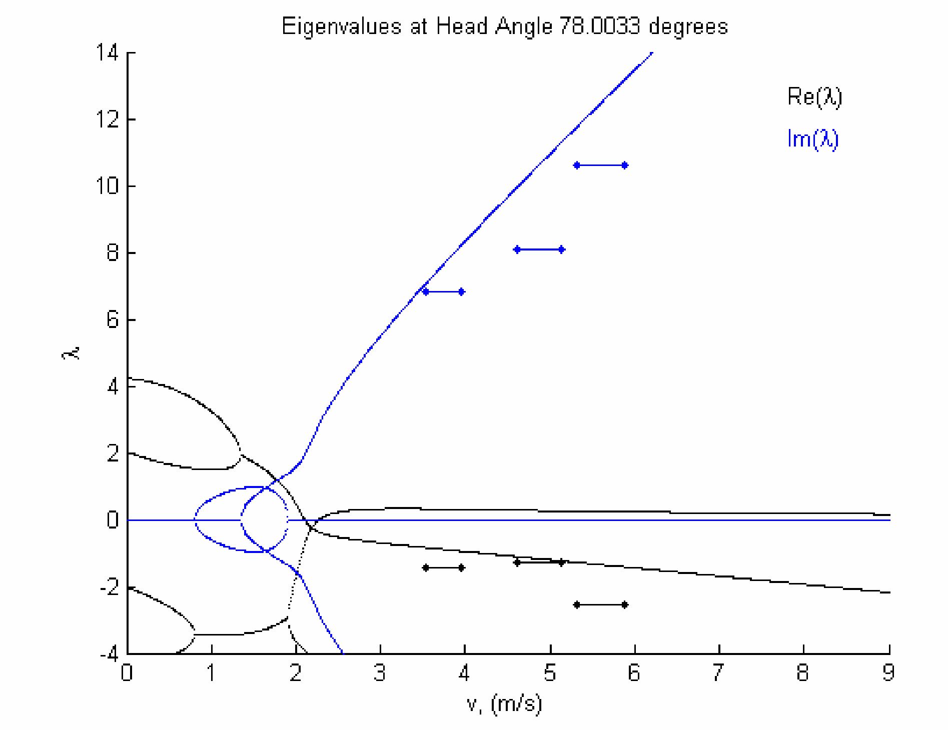

Figure 46: Experimental eigenvalues, head angle 78.0°.

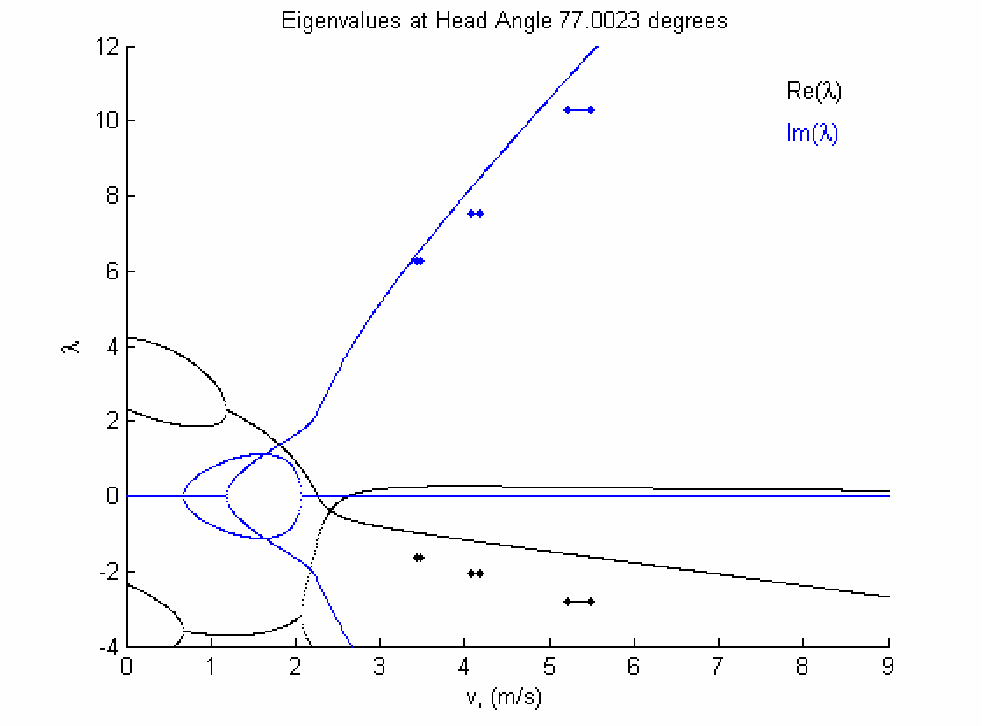

Figure 47: Experimental eigenvalues, head angle 77.0°.

For head angle 78° and 77°, in Figure 46, and Figure 47, results are similar. Relatively close fits are apparent for Im(λ), while experimental Re(λ) is observably more negative than predicted. Figure 46 shows less of a trend in experimental values. The lack of a true stable velocity region for these bicycle configurations, due to previously mentioned bifurcation of caster mode, may have a negative affect on results. These results also bring into question the method of curve fitting particularly over large velocity ranges. This will be discussed in more detail in subsequent chapters.

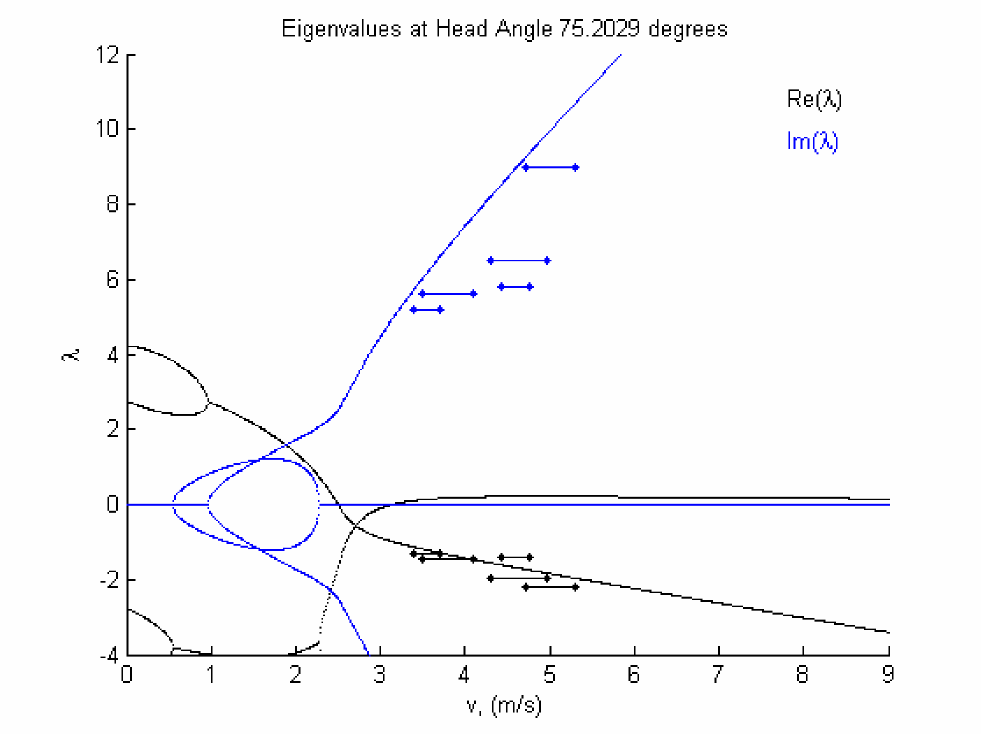

Figure 48: Experimental eigenvalues, head angle 75.2°.

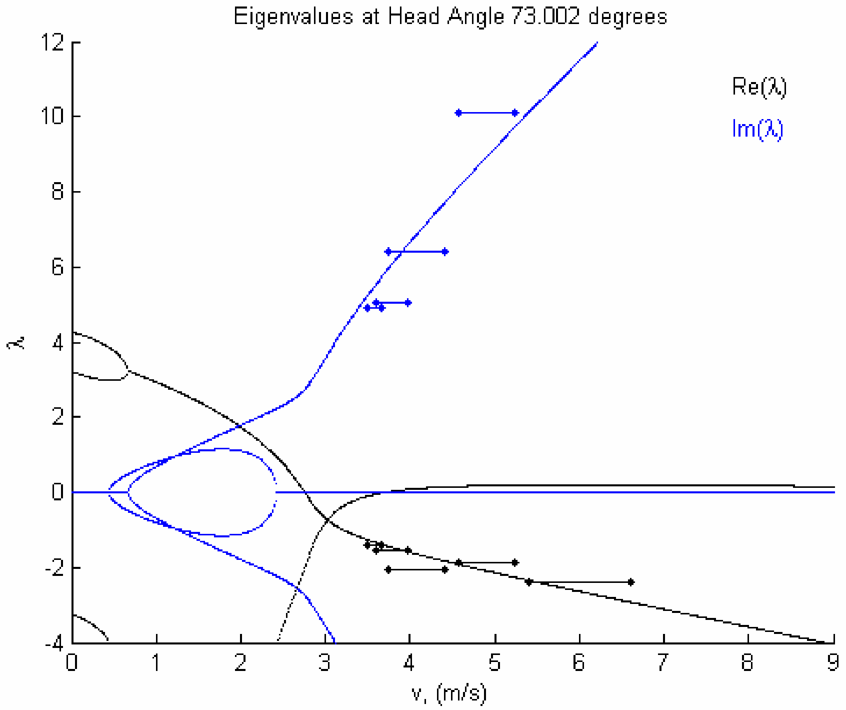

Figure 49: Experimental eigenvalues, head angle 73.0°.

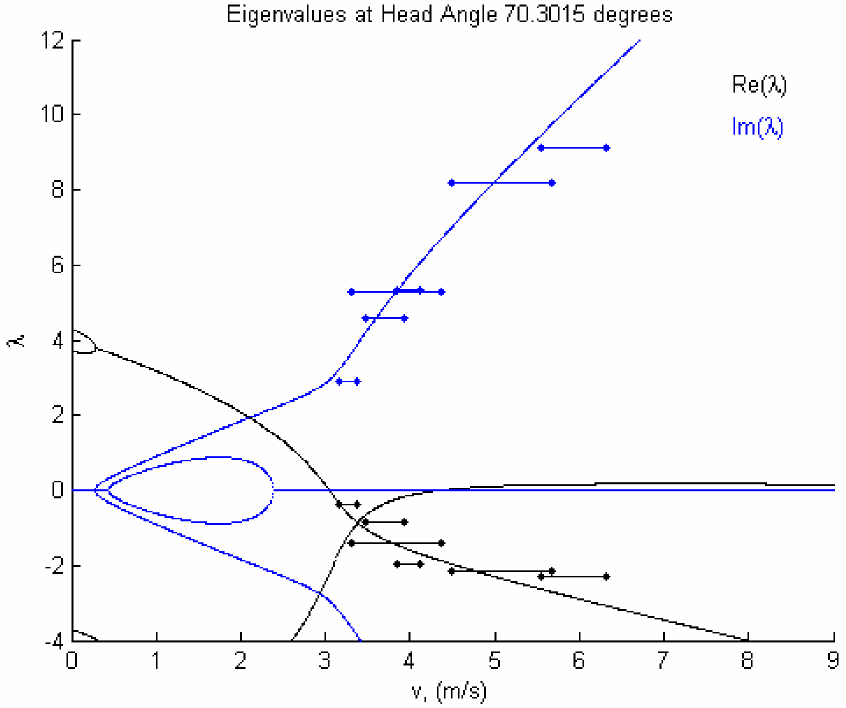

Figure 50: Experimental eigenvalues, head angle 70.3°.

For head angles 75.2°, 73.0°, and 70.3° (Figure 48, Figure 49, Figure 50), it was possible to capture more useful data at lower speeds. At these head angles, experimental eigenvalues showed strong relationships to those predicted with the linearized equations. Through observation, eigenvalues calculated at lower velocities show closer adherence to predicted results. There are still outlying results which do not fit the predicted curve, again bringing into question the curve fitting validity.

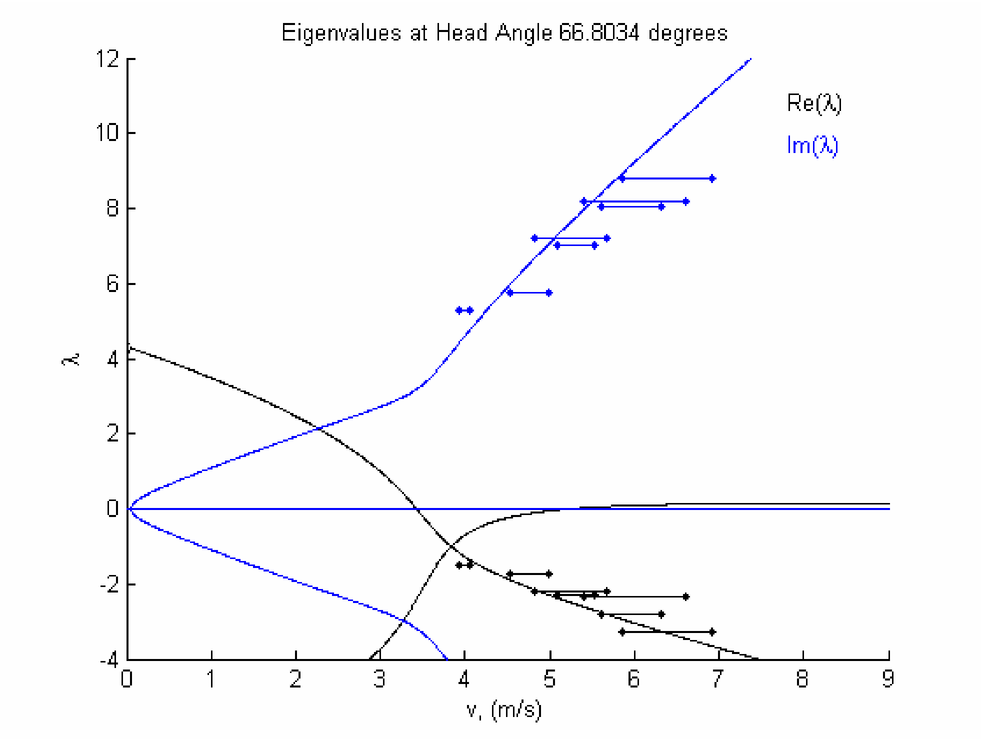

Figure 51: Experimental eigenvalues, head angle 66.8°.

The steepest head angle observed to display self stability in the subjective analysis process discussed earlier was 66.8°. This is also the steepest angle analyzed to display an independent capsize mode line from zero velocity, rather than one arising from saddle node bifurcation of the caster mode. Experimental results at this head angle show a smoother trend than results previously discussed for steeper head angles.

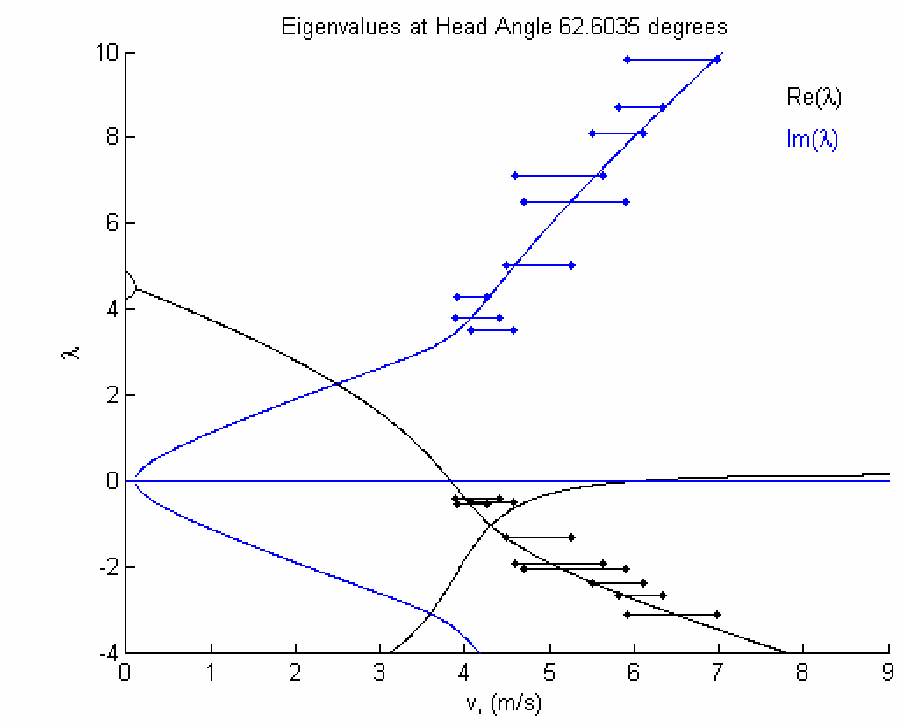

Figure 52: Experimental eigenvalues, head angle 62.6°.

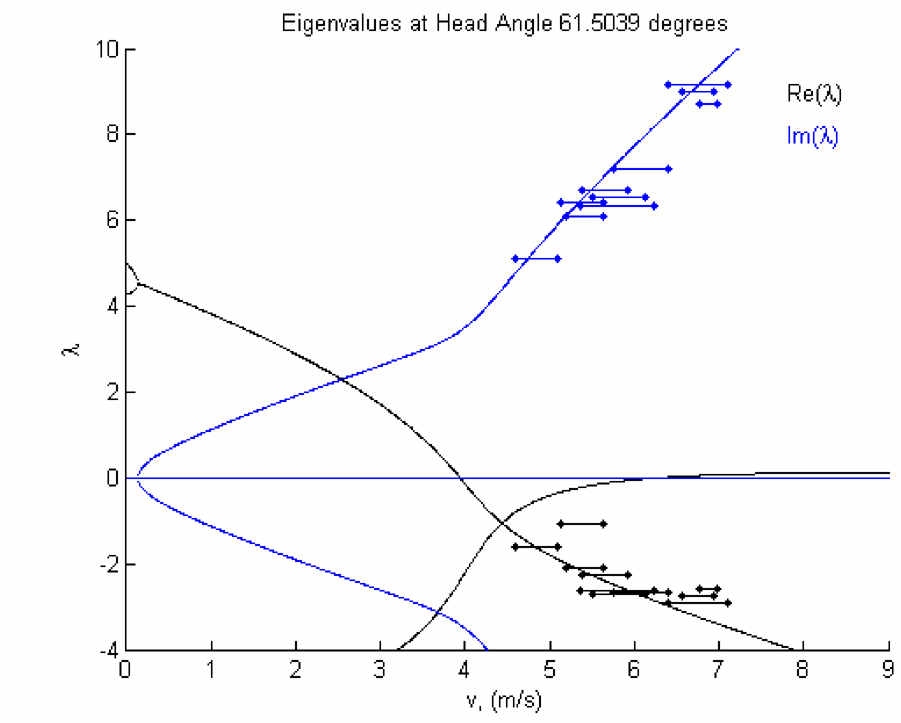

Figure 53: Experimental eigenvalues, head angle 61.5°.

For Figure 52 and Figure 53 results generally agree with predicted values. There is more discrepancy amongst data calculated over smaller velocity ranges. A small range gives limited data with which to fit a curve, leading to inaccuracies.

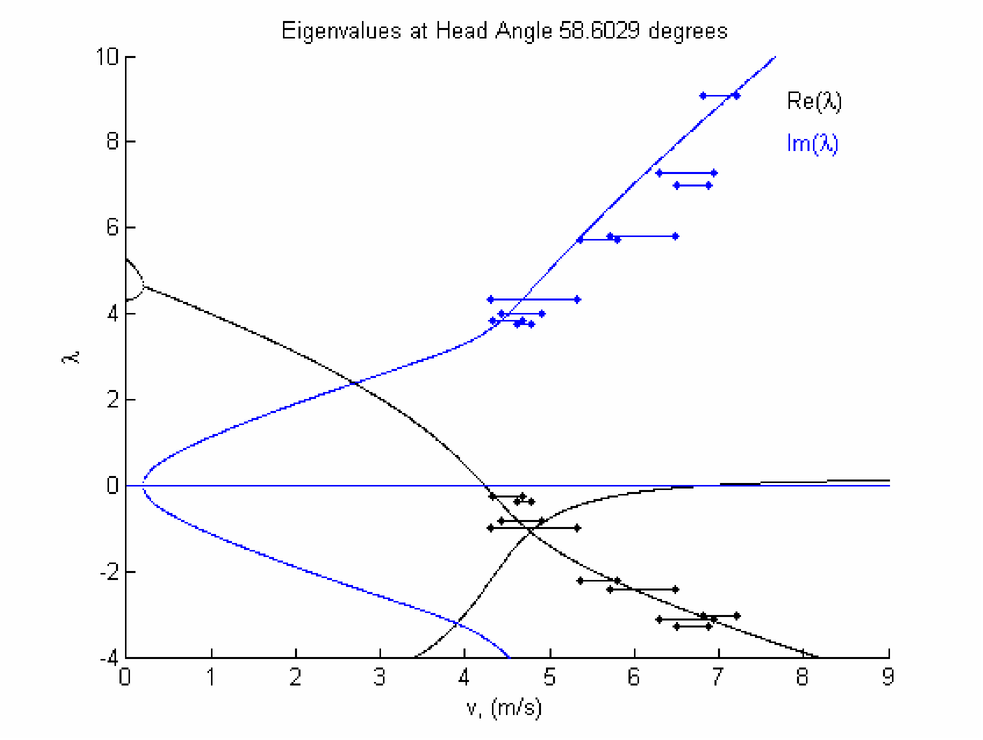

Figure 54: Experimental eigenvalues, head angle 58.6°.

In Figure 54, Figure 55, and it can be seen that with a lower head angle, and higher minimum stable speed, it was possible to calculate real eigenvalue parts very close to the x-axis. At higher speed the oscillations were more pronounced in the data, allowing a curve to be fitted close for velocities close to the lower stable region.

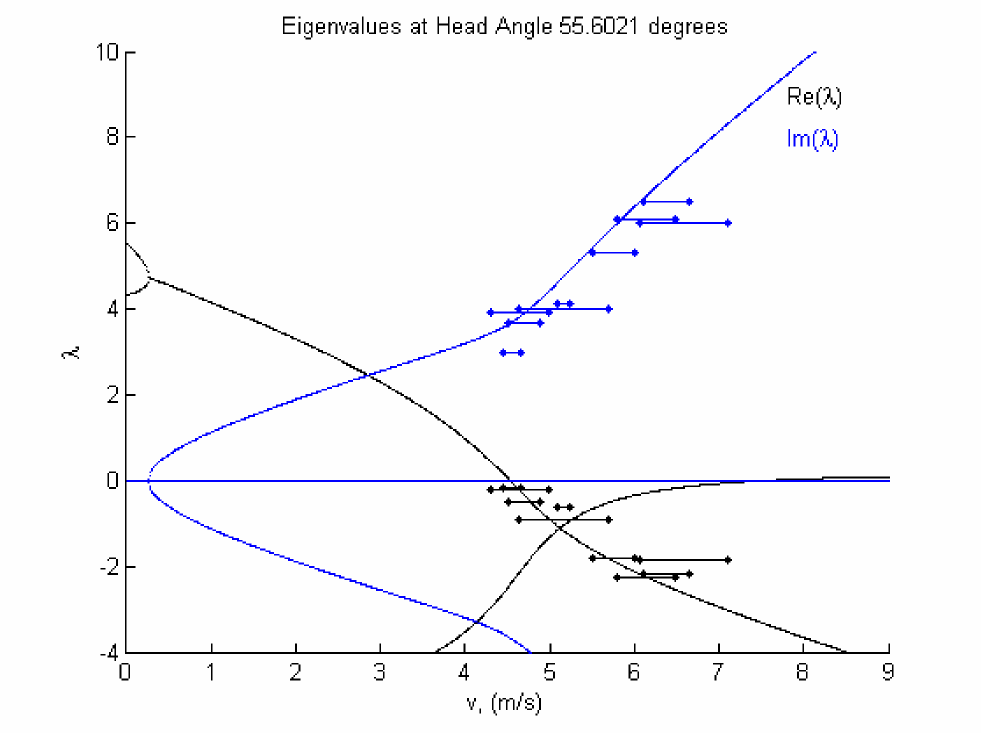

Figure 55: Experimental eigenvalues, head angle 55.6°.

8 Discussion of Results

The results gained through subjective observation, and experimental measurement show an agreement with those calculated using the linearized dynamics equations. The level of agreement varied through the range of head angles tested.

On initial inspection of results, the most unexpected aspect is the behaviour of caster and capsize modes. The bifurcation of these modes was not seen in study of previous literature. However, it is noted that during observations of the uncontrolled bicycle, self stability was not present until the head angle was lowered to 66.8°. This is also the highest angle at which caster and capsize modes were independent from zero velocity.

In conjunction with the knowledge that bifurcations increase instabilities of a dynamic system (Hunt et al, 2004), it may be hypothesized that the bicycle will not be stable with the capsize mode emanating from the merged capsize-caster mode line, despite all negative real roots.

Results calculated from measured data followed the same trends as the predicted results, with considerable spread. It is clear that there is agreement across all head angles tested, although there is some conflict at higher head angles, particularly above 66.8°. At the highest angles, difficulty was experienced in collecting useable data. The bicycle was most stable, although still in capsize, at higher speeds, and it was difficult to induce an oscillation without the bike turning sharply, at the risk of flipping. At lower, less stable speeds, it was not possible to start oscillations. The bicycle would simply fall in the direction it was pushed.

Accuracy of calculated results is questionable due to the curve fitting process. In some measured data, the resting values before and after oscillation were not equal. In most cases the differences were relatively small, compared to magnitude of oscillations, however, in some cases they were significant. The general equation that was used for curve fitting may need to have a second exponential component to be added, to account for this apparent drift. An example of this situation is seen in the steer angle data from Figure 41, between 2.5 and 6 seconds.

Another fundamental aspect of the curve fitting process is the calculation of eigenvalues over a range of velocities. The data oscillation curve is not truly of the form $y = e^{d(x)}\ (c_2 \cos(\omega x) + c_3 \sin(\omega x)) + c_1$, because the parameters vary with velocity. For example, the bicycle will have a lower weave frequency at a low velocity than it will at a high velocity, as such ω will be different for different velocities. Calculation of ω over a range of velocities can only result in a compromise, rather than an exact value. This holds for all coefficients. If the bicycle maintained steady velocity over the period of the oscillation, the technique would be accurate.

9 Conclusions and Recommendations for Future Work

This project provided experimental verification of the work of Meijaard, et al (2006). Previous levels of experimentation were surpassed, through testing on a range realistic bicycle configurations which modeled popular modern designs.

A bicycle for use in further experimentation has been designed, built, and successfully used, with variable head tube angle, and instrumentation to record motion.

The use of precision modeling in Pro Engineer to provide mass properties for complex systems has been demonstrated successfully.

The process of extracting eigenvalues from measured dynamics data has been applied, with accuracy sufficient to the needs of the project. However, flaws in the process have been discovered, and refinement in this area is suggested in continued investigations.

The techniques of this thesis may be used in the investigation of other design parameters, such as mass, wheel base, trail etc.

A useful continuation would be in the refinement of the test bicycle to include adjustable fork rake, with the aim of holding trail constant while varying head angle, or vice versa. In the same way, frame length could be made variable to hold wheel base constant.

Overall, this project was successful in demonstrating the applicability of the linearized dynamics equations of motions, to variations in popular design configurations seen on today's market.

10 Bibliography

Achelis S. B., 2001 *Technical analysis from A to Z*, McGraw Hill, New York

Astrom, K.J., Klein, R.E. & Lennartsson, A. 2005 *Bicycle dynamics and control: Adapted bicycles for education and research*. IEEE Control Systems Magazine 25(4), 26–47.

Encyclopædia Britannica 2009, *Mechanics*. from Encyclopædia Britannica Online: http://www.britannica.com/EBchecked/topic/371907/mechanics

Guckenheimer, J., (2007) *Bifurcation*. Scholarpedia, 2(6):1517

Hassard, B. D., Nicholas D. 1981 *Theory and applications of Hopf bifurcation*, University of Cambridge Press, Cambridge

Herlihy D. V., 2004, *Bicycle*, Yale University Press, London

Hunt, B. R., Kennedy, J. A., Li, T-Y., 2004, *The theory of chaotic attractors*, Springer – Verlag, New York

Jones, David E., 1970, *The Stability of the Bicycle*, Physics Today, 23 (3), Re-issued September 2006, 59, 9, pp. 51–56

Klein, F. & Sommerfeld, A. 1910 ¨ Uber die Theorie des Kreisels, Ch. IX, Section 8, Stabilit at des Fahrrads,' (English translation http://ruina.tam.cornell.edu/research.)

Kooijman J. D., Schwab, A.L., J.P. Meijaard, J.P., 2006. *Experimental Validation of a Model for the Motion of an Uncontrolled Bicycle*, Multibody Syst Dyn (2008) 19: 115–132, Springer Science+Business Media, Inc.

Meijaard, J. P., Papadopoulos, J. M., Ruina, A., Schwab, A. L., *Linearized dynamics equations for the balance and steer of a bicycle: a benchmark and review* PRS Series 1

Ne˘ımark, Ju. I. & Fufaev, N. A. 1972 *Dynamics of Nonholonomic Systems*. Providence, RI (Transl. from the Russian edition, Nauka, Moscow, 1967.)

Papadopoulos, J. M. 1987 *Bicycle steering dynamics and self-stability: A summary report on work in progress*. Technical report, Cornell Bicycle Research Project, Cornell University

Paterek, T., 1985, *The Paterek Manual for Bicycle Frame Builders,* Kermesse Distributor Inc., PA.

Psiaki, M. L. 1979 *Bicycle stability: A mathematical and numerical analysis*. Undergradute thesis, Physics Dept., Princeton University, NJ.

Rankine, W. J. M. 1869, *On the dynamical principles of the motion of velocipedes*. The Engineer 28, (1870), http://tam.cornell.edu/ als93/

Rice, R. S. & Roland, R.D. 1970 *An evaluation of the performance and handling qualities of bicycles.* Calspan Report VJ-2888-K

Sharp, A. 1896 *Bicycles and tricycles; an elementary treatise on their design and construction*, London: Longmans Green.

Sharp, R. S. 1971 *The stability and control of motorcycles*. Journal of Mechanical Engineering Science 13(5)

Weisstein, E. W., *Damped Simple Harmonic Motion--Underdamping*. From MathWorld--A Wolfram Web Resource. http://mathworld.wolfram.com/DampedSimpleHarmonicMotionUnderdamping.html

Weisstein, E. W., *Logistic Map*. From MathWorld--A Wolfram Web Resource. http://mathworld.wolfram.com/LogisticMap.html

Whipple, F. J. W. 1899 *The Stability of the Motion of a Bicycle*. The Quarterly Journalof Pure and Applied Mathematics 30,

Wilson, D. G., Papadopoulos, J., Whitt F. H., 2004 *Bicycling science*, The MIT Press, Massachusetts

11 Appendix

11.1 Appendix A: Calculation of Coefficients of Linearized Dynamics Equation

Taken from “Linearized Dynamics Equations for the Balance and Steer of a Bicycle: A Benchmark and Review”, J. P. Meijaard, J. M. Papadopoulos, A. Ruina and A. L. Schwab, 2006.

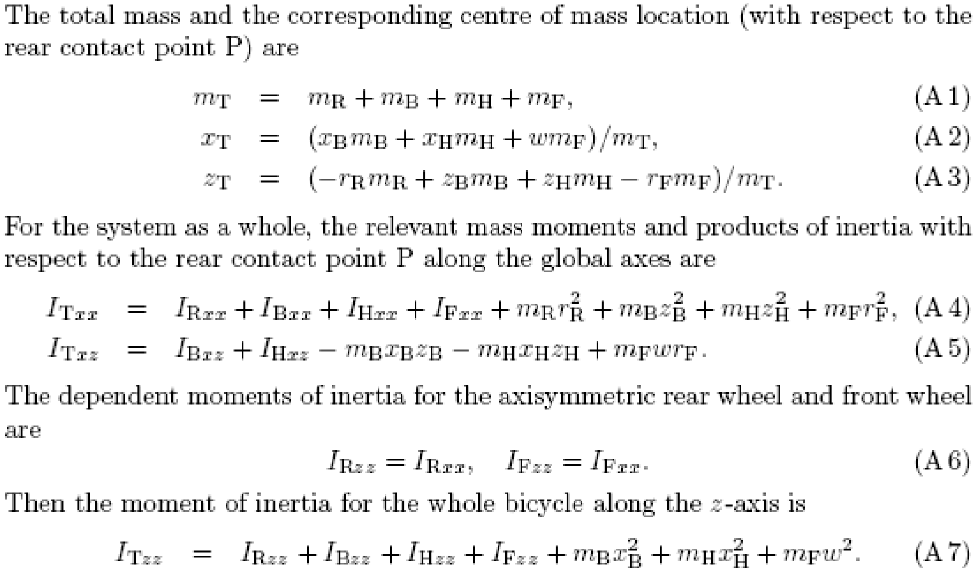

The total mass and the corresponding centre of mass location (with respect to the rear contact point P) are

$$
\begin{aligned}
m_{\mathrm{T}} &= m_{\mathrm{R}} + m_{\mathrm{B}} + m_{\mathrm{H}} + m_{\mathrm{F}}, && \text{(A 1)}\\
x_{\mathrm{T}} &= (x_{\mathrm{B}} m_{\mathrm{B}} + x_{\mathrm{H}} m_{\mathrm{H}} + w m_{\mathrm{F}})/m_{\mathrm{T}}, && \text{(A 2)}\\
z_{\mathrm{T}} &= (-r_{\mathrm{R}} m_{\mathrm{R}} + z_{\mathrm{B}} m_{\mathrm{B}} + z_{\mathrm{H}} m_{\mathrm{H}} - r_{\mathrm{F}} m_{\mathrm{F}})/m_{\mathrm{T}}. && \text{(A 3)}
\end{aligned}
$$

For the system as a whole, the relevant mass moments and products of inertia with respect to the rear contact point P along the global axes are

$$
\begin{aligned}
I_{\mathrm{T}xx} &= I_{\mathrm{R}xx} + I_{\mathrm{B}xx} + I_{\mathrm{H}xx} + I_{\mathrm{F}xx} + m_{\mathrm{R}} r_{\mathrm{R}}^2 + m_{\mathrm{B}} z_{\mathrm{B}}^2 + m_{\mathrm{H}} z_{\mathrm{H}}^2 + m_{\mathrm{F}} r_{\mathrm{F}}^2, && \text{(A 4)}\\
I_{\mathrm{T}xz} &= I_{\mathrm{B}xz} + I_{\mathrm{H}xz} - m_{\mathrm{B}} x_{\mathrm{B}} z_{\mathrm{B}} - m_{\mathrm{H}} x_{\mathrm{H}} z_{\mathrm{H}} + m_{\mathrm{F}} w r_{\mathrm{F}}. && \text{(A 5)}
\end{aligned}
$$

The dependent moments of inertia for the axisymmetric rear wheel and front wheel are

$$
I_{\mathrm{R}zz} = I_{\mathrm{R}xx}, \quad I_{\mathrm{F}zz} = I_{\mathrm{F}xx}. \qquad \text{(A 6)}
$$

Then the moment of inertia for the whole bicycle along the z-axis is

$$
I_{\mathrm{T}zz} = I_{\mathrm{R}zz} + I_{\mathrm{B}zz} + I_{\mathrm{H}zz} + I_{\mathrm{F}zz} + m_{\mathrm{B}} x_{\mathrm{B}}^2 + m_{\mathrm{H}} x_{\mathrm{H}}^2 + m_{\mathrm{F}} w^2. \qquad \text{(A 7)}
$$

The same properties are similarly defined for the front assembly A:

$$m_{\rm A} = m_{\rm H} + m_{\rm F}, \tag{A 8}$$

$$x_{\rm A} = (x_{\rm H}m_{\rm H} + wm_{\rm F})/m_{\rm A}, \qquad z_{\rm A} = (z_{\rm H}m_{\rm H} - r_{\rm F}m_{\rm F})/m_{\rm A}. \tag{A 9}$$

The relevant mass moments and products of inertia for the front assembly with respect to the centre of mass of the front assembly along the global axes are

$$\begin{aligned} I_{{\rm A}xx} &= I_{{\rm H}xx} + I_{{\rm F}xx} + m_{\rm H}(z_{\rm H} - z_{\rm A})^2 + m_{\rm F}(r_{\rm F} + z_{\rm A})^2, & \text{(A 10)}\\ I_{{\rm A}xz} &= I_{{\rm H}xz} - m_{\rm H}(x_{\rm H} - x_{\rm A})(z_{\rm H} - z_{\rm A}) + m_{\rm F}(w - x_{\rm A})(r_{\rm F} + z_{\rm A}), & \text{(A 11)}\\ I_{{\rm A}zz} &= I_{{\rm H}zz} + I_{{\rm F}zz} + m_{\rm H}(x_{\rm H} - x_{\rm A})^2 + m_{\rm F}(w - x_{\rm A})^2. & \text{(A 12)} \end{aligned}$$

Let $\boldsymbol{\lambda} = (\sin\lambda, 0, \cos\lambda)^T$ be a unit vector pointing down along the steer axis where λ is the angle in the xz-plane between the downward steering axis and the $+z$ direction. The centre of mass of the front assembly is ahead of the steering axis by perpendicular distance

$$u_{\rm A} = (x_{\rm A} - w - c)\cos\lambda - z_{\rm A}\sin\lambda. \tag{A 13}$$

For the front assembly three special inertia quantities are needed: the moment of inertia about the steer axis and the products of inertia relative to crossed, skew axes, taken about the points where they intersect. The latter give the torque about one axis due to angular acceleration about the other. For example, the λx component is taken about the point where the steer axis intersects the ground plane. It includes a part from I_A operating on unit vectors along the steer axis and along x, and also a parallel axis term based on the distance of m_A from each of those axes.

$$\begin{aligned} I_{{\rm A}\lambda\lambda} &= m_{\rm A}u_{\rm A}^2 + I_{{\rm A}xx}\sin^2\lambda + 2I_{{\rm A}xz}\sin\lambda\cos\lambda + I_{{\rm A}zz}\cos^2\lambda, & \text{(A 14)}\\ I_{{\rm A}\lambda x} &= -m_{\rm A}u_{\rm A}z_{\rm A} + I_{{\rm A}xx}\sin\lambda + I_{{\rm A}xz}\cos\lambda, & \text{(A 15)}\\ I_{{\rm A}\lambda z} &= m_{\rm A}u_{\rm A}x_{\rm A} + I_{{\rm A}xz}\sin\lambda + I_{{\rm A}zz}\cos\lambda. & \text{(A 16)} \end{aligned}$$

The ratio of the mechanical trail (i.e., the perpendicular distance that the front wheel contact point is behind the steering axis) to the wheel base is

$$\mu = (c/w)\cos\lambda. \tag{A 17}$$

The rear and front wheel angular momenta along the y-axis, divided by the forward speed, together with their sum form the gyrostatic coefficients:

$$S_{\rm R} = I_{{\rm R}yy}/r_{\rm R}, \quad S_{\rm F} = I_{{\rm F}yy}/r_{\rm F}, \quad S_{\rm T} = S_{\rm R} + S_{\rm F}. \tag{A 18}$$

We define a frequently appearing static moment term as

$$S_{\rm A} = m_{\rm A}u_{\rm A} + \mu m_{\rm T}x_{\rm T}. \tag{A 19}$$

The entries in the linearized equations of motion can now be formed. The mass moments of inertia

$$\begin{aligned} M_{\phi\phi} &= I_{{\rm T}xx} \quad , \quad M_{\phi\delta} = I_{{\rm A}\lambda x} + \mu I_{{\rm T}xz},\\ M_{\delta\phi} &= M_{\phi\delta} \quad , \quad M_{\delta\delta} = I_{{\rm A}\lambda\lambda} + 2\mu I_{{\rm A}\lambda z} + \mu^2 I_{{\rm T}zz}, \end{aligned} \tag{A 20}$$

are elements of the symmetric mass matrix $\mathbf{M} = \begin{bmatrix} M_{\phi\phi} & M_{\phi\delta} \\ M_{\delta\phi} & M_{\delta\delta} \end{bmatrix}$. (A 21)

The gravity-dependent stiffness terms (to be multiplied by g) are

$$\begin{aligned} K_{0\phi\phi} &= m_{\mathrm{T}} z_{\mathrm{T}} \quad , \quad K_{0\phi\delta} = -S_{\mathrm{A}}, \\ K_{0\delta\phi} &= K_{0\phi\delta} \quad , \quad K_{0\delta\delta} = -S_{\mathrm{A}} \sin\lambda, \end{aligned} \tag{A 22}$$

which form the stiffness matrix $\mathbf{K_0} = \begin{bmatrix} K_{0\phi\phi} & K_{0\phi\delta} \\ K_{0\delta\phi} & K_{0\delta\delta} \end{bmatrix}$. (A 23)

The velocity-dependent stiffness terms (to be multiplied by v^2) are

$$\begin{aligned} K_{2\phi\phi} &= 0 \quad , \quad K_{2\phi\delta} = ((S_{\mathrm{T}} - m_{\mathrm{T}} z_{\mathrm{T}})/w) \cos\lambda, \\ K_{2\delta\phi} &= 0 \quad , \quad K_{2\delta\delta} = ((S_{\mathrm{A}} + S_{\mathrm{F}} \sin\lambda)/w) \cos\lambda, \end{aligned} \tag{A 24}$$

which form the stiffness matrix $\mathbf{K_2} = \begin{bmatrix} K_{2\phi\phi} & K_{2\phi\delta} \\ K_{2\delta\phi} & K_{2\delta\delta} \end{bmatrix}$. (A 25)

In the equations we use $\mathbf{K} = g\mathbf{K_0} + v^2\mathbf{K_2}$. Finally the "damping" terms are

$$C_{1\phi\phi} = 0, \quad C_{1\phi\delta} = \mu S_{\mathrm{T}} + S_{\mathrm{F}} \cos\lambda + (I_{\mathrm{T}xz}/w) \cos\lambda - \mu m_{\mathrm{T}} z_{\mathrm{T}}, \tag{A 26}$$

$$C_{1\delta\phi} = -(\mu S_{\mathrm{T}} + S_{\mathrm{F}} \cos\lambda), \quad C_{1\delta\delta} = (I_{\mathrm{A}\lambda z}/w) \cos\lambda + \mu(S_{\mathrm{A}} + (I_{\mathrm{T}zz}/w) \cos\lambda),$$

which form $\mathbf{C_1} = \begin{bmatrix} C_{1\phi\phi} & C_{1\phi\delta} \\ C_{1\delta\phi} & C_{1\delta\delta} \end{bmatrix}$ where we use $\mathbf{C} = v\mathbf{C_1}$. (A 27)

11.2 Appendix B: Calculated coefficients for tested head angles

Head Angle = 81.9019°

$$\mathbf{M} = \begin{matrix} 3.194496 & -0.00573 \\ -0.00573 & 0.054038 \end{matrix}$$

$$\mathbf{C} = \begin{matrix} 0 & 3.080122 \\ -0.29721 & 0.080084 \end{matrix}$$

$$\mathbf{K_0} = \begin{matrix} -56.2981 & -0.05879 \\ -0.05879 & -0.00828 \end{matrix}$$

$$\mathbf{K_2} = \begin{matrix} 0 & 6.235084 \\ 0 & 0.048741 \end{matrix}$$

Head Angle = 80.8007°

$$\mathbf{M} = \begin{matrix} 3.179155 & 0.012961 \\ 0.012961 & 0.055174 \end{matrix}$$

$$\mathbf{C} = \begin{matrix} 0 & 3.083171 \\ -0.30007 & 0.109574 \end{matrix}$$

$$\mathbf{K_0} = \begin{matrix} -56.1527 & -0.42952 \\ -0.42952 & -0.06867 \end{matrix}$$

$$\mathbf{K_2} = \begin{matrix} 0 & 6.139038 \\ 0 & 0.090374 \end{matrix}$$

Head Angle = 79.0046°

$$\mathbf{M} = \begin{matrix} 3.179155 & 0.037993 \\ 0.037993 & 0.057571 \end{matrix}$$

$$\mathbf{C} = \begin{matrix} 0 & 3.088251 \\ -0.30431 & 0.14778 \end{matrix}$$

$$\mathbf{K_0} = \begin{matrix} -56.1527 & -0.92982 \\ -0.92982 & -0.17735 \end{matrix}$$

$$\mathbf{K_2} = \begin{matrix} 0 & 6.004686 \\ 0 & 0.145728 \end{matrix}$$

Head Angle = 78.0033°

$$\mathbf{M} \quad \begin{matrix} 3.120361 & 0.0559 \\ 0.0559 & 0.059499 \end{matrix}$$

$$\mathbf{C} \quad \begin{matrix} 0 & 3.059045 \\ -0.30641 & 0.179224 \end{matrix}$$

$$\mathbf{K_0} \quad \begin{matrix} -55.5908 & -1.30214 \\ -1.30214 & -0.27066 \end{matrix}$$

$$\mathbf{K_2} \quad \begin{matrix} 0 & 5.822763 \\ 0 & 0.18267 \end{matrix}$$

Head Angle = 77.0023°

$$\mathbf{M} = \begin{matrix} 3.120361 & 0.074534 \\ 0.074534 & 0.061573 \end{matrix}$$

$$\mathbf{C} = \begin{matrix} 0 & 3.079416 \\ -0.30841 & 0.20775 \end{matrix}$$

$$\mathbf{K_0} = \begin{matrix} -55.5908 & -1.66767 \\ -1.66767 & -0.37508 \end{matrix}$$

$$\mathbf{K_2} = \begin{matrix} 0 & 5.800259 \\ 0 & 0.221221 \end{matrix}$$

Head Angle = 75.2029°

$$\mathbf{M} = \begin{matrix} 3.089471 & 0.102119 \\ 0.102119 & 0.06583 \end{matrix}$$

$$\mathbf{C} = \begin{matrix} 0 & 3.070224 \\ -0.31154 & 0.252119 \end{matrix}$$

$$\mathbf{K_0} = \begin{matrix} -55.2927 & -2.23263 \\ -2.23263 & -0.57021 \end{matrix}$$

$$\mathbf{K_2} = \begin{matrix} 0 & 5.63661 \\ 0 & 0.276426 \end{matrix}$$

Head Angle = 73.002°

$$\mathbf{M} = \begin{matrix} 3.049195 & 0.134455 \\ 0.134455 & 0.071991 \end{matrix}$$

$$\mathbf{C} = \begin{matrix} 0 & 3.0528 \\ -0.31468 & 0.304298 \end{matrix}$$

$$\mathbf{K_0} = \begin{matrix} -54.9009 & -2.90503 \\ -2.90503 & -0.84925 \end{matrix}$$

$$\mathbf{K_2} = \begin{matrix} 0 & 5.434465 \\ 0 & 0.33816 \end{matrix}$$

Head Angle = 70.3015°

$$\mathbf{M} = \begin{matrix} 2.996243 & 0.17203 \\ 0.17203 & 0.080847 \end{matrix}$$

$$\mathbf{C} = \begin{matrix} 0 & 3.022605 \\ -0.31751 & 0.364965 \end{matrix}$$

$$\mathbf{K_0} = \begin{matrix} -54.3801 & -3.70275 \\ -3.70275 & -1.24809 \end{matrix}$$

$$\mathbf{K_2} = \begin{matrix} 0 & 5.184537 \\ 0 & 0.405459 \end{matrix}$$

Head Angle = 66.8034°

$$\mathbf{M} = \begin{matrix} 3.134634 & 0.23016 \\ 0.23016 & 0.095152 \end{matrix}$$

$$\mathbf{C} = \begin{matrix} 0 & 3.207847 \\ -0.31955 & 0.451808 \end{matrix}$$

$$\mathbf{K_0} = \begin{matrix} -56.6206 & -4.87317 \\ -4.87317 & -1.91948 \end{matrix}$$

$$\mathbf{K_2} = \begin{matrix} 0 & 5.101766 \\ 0 & 0.494024 \end{matrix}$$

Head Angle = 62.6035°

$$\mathbf{M} = \begin{matrix} 2.826624 & 0.266375 \\ 0.266375 & 0.112444 \end{matrix}$$

$$\mathbf{C} = \begin{matrix} 0 & 2.888107 \\ -0.31967 & 0.51522 \end{matrix}$$

$$\mathbf{K_0} = \begin{matrix} -52.6654 & -5.81499 \\ -5.81499 & -2.67574 \end{matrix}$$

$$\mathbf{K_2} = \begin{matrix} 0 & 4.470078 \\ 0 & 0.548996 \end{matrix}$$

Head Angle = 61.5039°

$$\mathbf{M} = \begin{matrix} 2.800453 & 0.278311 \\ 0.278311 & 0.117569 \end{matrix}$$

$$\mathbf{C} = \begin{matrix} 0 & 2.863598 \\ -0.31929 & 0.53372 \end{matrix}$$

$$\mathbf{K_0} = \begin{matrix} -52.3941 & -6.09746 \\ -6.09746 & -2.90909 \end{matrix}$$

$$\mathbf{K_2} = \begin{matrix} 0 & 4.368701 \\ 0 & 0.563991 \end{matrix}$$

Head Angle = 58.6029°

$$\mathbf{M} = \begin{matrix} 2.729476 & 0.307965 \\ 0.307965 & 0.131643 \end{matrix}$$

$$\mathbf{C} = \begin{matrix} 0 & 2.793277 \\ -0.31752 & 0.578756 \end{matrix}$$

$$\mathbf{K_0} = \begin{matrix} -51.6483 & -6.81989 \\ -6.81989 & -3.55293 \end{matrix}$$

$$\mathbf{K_2} = \begin{matrix} 0 & 4.103026 \\ 0 & 0.597364 \end{matrix}$$

11.3 Appendix C Drawings

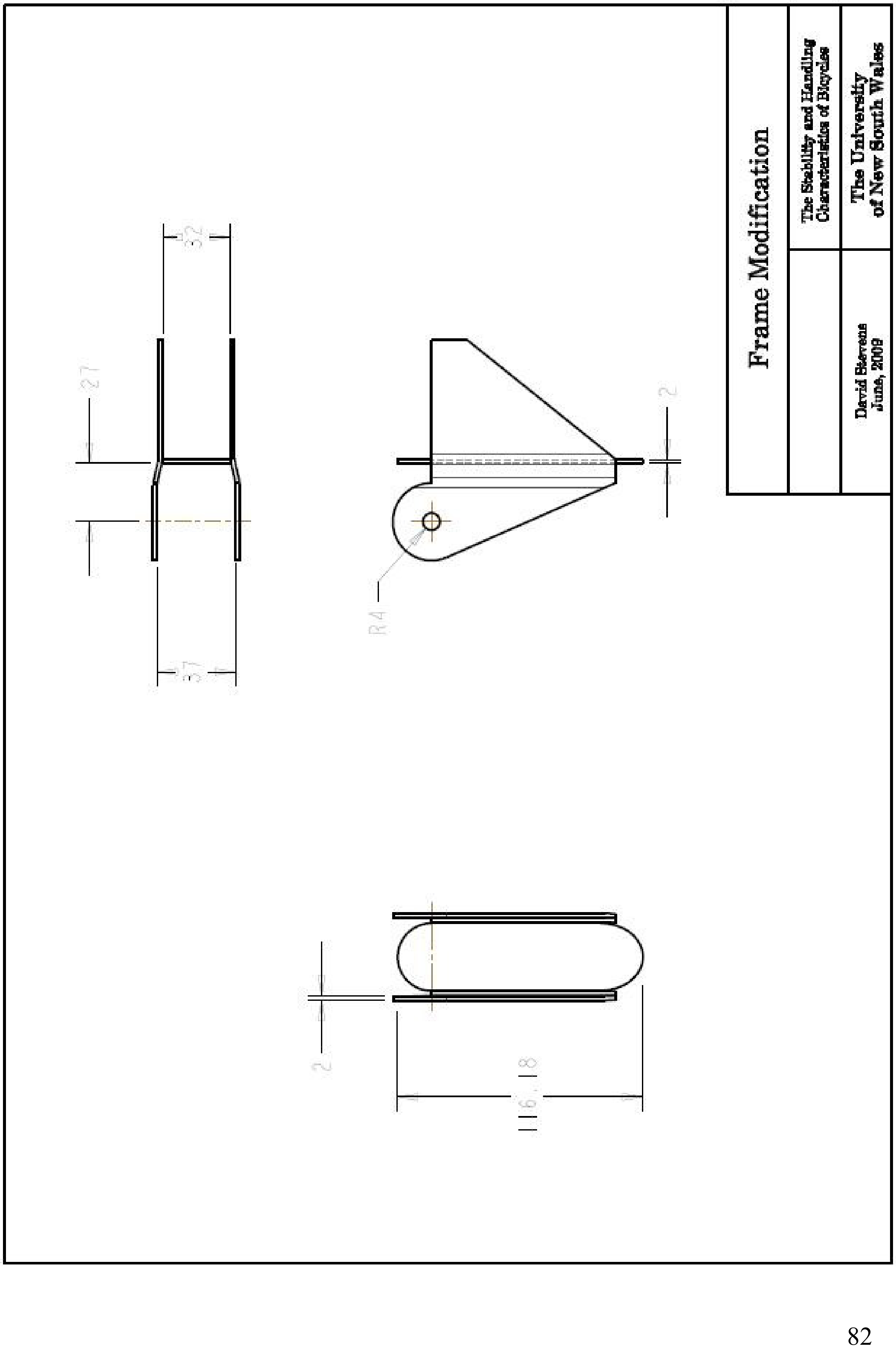

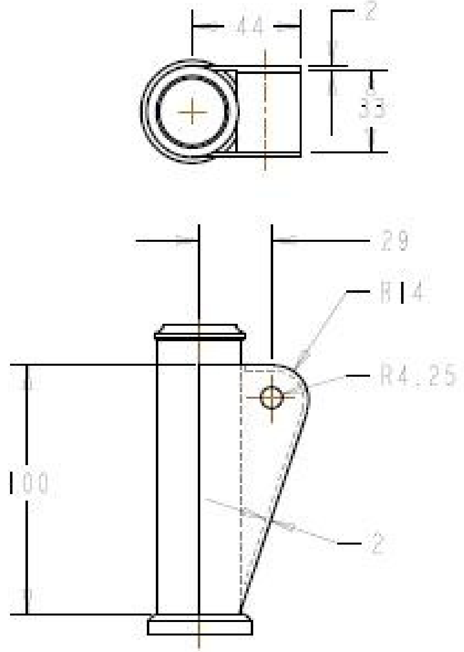

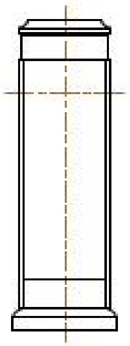

Head Tube Modification

The Stability and Handling
Characteristics of Bicycles

David Stevens
June, 2009

The University
of New South Wales

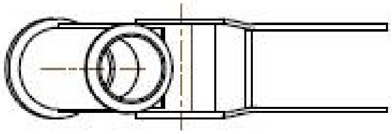

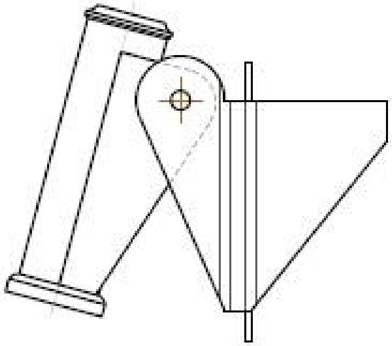

Variable Head Tube Assembly

The Stability and Handling
Characteristics of Bicycles

David Stevens
June, 2009

The University
of New South Wales